Sustainable Cities and Society 91 (2023) 104433

Contents lists available at ScienceDirect

Sustainable Cities and Society

journal homepage: www.elsevier.com/locate/scs

# Compound daytime and nighttime heatwaves for air and surface temperature based on relative and absolute threshold dynamic classified in Southwest China, 1980–2019

Qingping Cheng [a,b,c,*], Hanyu Jin [a], Yitong Ren [a]

[a] School of Geography and Ecotourism, Southwest Forestry University, Kunming 650224, China
[b] Southwest Research Centre for Eco-Civilization, National Forestry and Grassland Administration, Kunming 650224, China
[c] National (Yunnan Province) Field Science Observation and Research Station Yulong Snow Mountain Cryosphere and Sustainable Development, Northwest Institute of Eco-Environment and Resources, Chinese Academy of Sciences, Lanzhou 730000, China

ARTICLE INFO

*Keywords:*
Air and surface temperature heatwaves
Relative and absolute thresholds
Dynamic classifications
Urbanization impact
Southwest China

ABSTRACT

Heatwaves pose potential risks to the environment, energy, society, and public health, and compound daytime and nighttime air and surface temperature heatwaves have the most severe effects. In this study, Southwest China was taken as a case to explore the characteristics of daytime, nighttime, and concurrent daytime and nighttime heatwaves events using air and surface temperatures based on a dynamic method for classifying urban, suburban, and rural stations with 30 m resolution land use and cover data based on absolute (i.e., same threshold for the entire Southwest China) and relative thresholds (i.e., thresholds for Chongqing municipality, Sichuan, Yunnan, and Guizhou Provinces calculated separately based on built-up areas for each period). We found that heatwaves events became more frequent and more severe in urban, suburban, and rural areas based on absolute and relative thresholds for both air and surface temperatures. Overall, the positive contributions towards warming by urbanization in urban and suburban areas to different heatwaves events obviously differed among different buffer areas and the influence of urbanization was different for air and surface temperature heatwaves events based on absolute and relative thresholds. Spatially persistent compound heatwaves mainly occurred in three urban agglomerations for air temperature. This study provides an original research perspective by using air and surface temperatures during daytime, nighttime, and concurrent daytime and nighttime heatwaves to calculate indices based on absolute (fixed threshold) and relative thresholds (considering the social and economic development level of different regions) in the complex topography of the Southwest China. In addition, this study observed for the first time that the calculated heatwaves indices based on air and surface temperatures were obviously different, illustrating that results obtained using different data sources (e.g., air temperature, surface temperature, and remote sensing data) to evaluate heatwaves will differ, indicating that data sources need to be carefully considered in Southwest China and other regions.

## 1. Introduction

As one of the sustainable development goals of the United Nations, sustainable cities and communities play a key role in the overall realization of the United Nations sustainable development goals. As significant hubs of human activity and interaction, cities have undergone major changes in their atmosphere and surface temperatures as a result of population increases and increased spread of impervious surfaces (He et al., 2021; Jamei et al., 2019), which alters the properties of the atmospheric boundary layer and impacts weather conditions in urban areas (Chuan et al., 2022). Heatwaves, which pose potential threats to public health, food security, energy production and distribution, and ecosystem sustainability, are more obvious in cities and are becoming increasingly common in various regions of the world as climates warm (Christidis et al., 2015; Frölicher et al., 2018; Shi, et al., 2021; Wang et al., 2021a, 2021b; Wu et al., 2020; Zhang et al., 2020). In recently years, heatwaves patterns in the 21st century have been extensively studied in various regions (cities) and on various scales, including the Northern Hemisphere (Vogel et al., 2019; Wang et al., 2020), Europe (Christidis et al., 2015; Larcom et al., 2019), America (Rastogi et al.,

* Corresponding author at: School of Geography and Ecotourism, Southwest Forestry University, Kunming 650224, China.
*E-mail address:* qpchengtyli@foxmail.com (Q. Cheng).

https://doi.org/10.1016/j.scs.2023.104433
Received 2 July 2022; Received in revised form 10 December 2022; Accepted 27 January 2023
Available online 30 January 2023

2020), India (Panda et al., 2017), France (Todd & Valleron, 2015), Finland (Ruuhela et al., 2018), South Korea (Kim et al., 2019), and globally (Chen et al., 2020; Ma et al., 2021; Yin et al., 2019). Moreover, more intense, longer lasting, more frequent, and more impactful heatwaves are anticipated in the 21st century as anthropogenic warming substantially increases (Chen et al., 2015, 2020; Russo et al., 2014). Furthermore, rapid urbanization in the developing world over recent decades has exacerbated the warming of urban environments due to the urban heat island effect, which are present no matter the size, latitude, coastal, inland position, topography, or local environment of a city (Arnfield, 2003). Heat island effects are rapidly increasing health risks within cities due to the fast-paced growth of urban populations (Manoli et al., 2019) and urban economies. In view of the serious impacts of high temperature related events (heat island, heatwaves, hot pressure, etc.) on the ecological environment and social economy, studying these events has always been a hot topic globally (Varentsov et al., 2019; Zhao, 2018). Therefore, as one of the most obvious high temperature events, it is important to reveal the temporal and spatial variation characteristics of heatwaves and the expected impact of urbanization to provide a theoretical framework for urban planners and urban residents to take relevant measures (such as green roofs and cool roofs) to adapt to the increasing urban heatwaves.

As the world's largest developing country, heatwaves in China have become more frequent and severe since the mid-1990s. According to the most recent Lancet Countdown report, the number of deaths in China due to heatwaves increased by a factor of four between 1990 and 2019, reaching 26,800 deaths (Cai et al., 2020). With significant decadal increases in daytime (DYT), nighttime (NGT), and concurrent (CDNG; both DYT and NGT) heatwaves which have featured rapid increases in frequency, intensity, and spatial extent (Su & Dong, 2019a, b). Furthermore, relative to present day, the DYT, NGT, and CDNG heatwaves over China are projected to become more frequent with higher intensities and elongated durations under the RCP4.5 scenario (Su & Dong, 2019a). In recent decades, several record-breaking heatwaves events have occurred in China (Kong et al., 2020), including in August of 2003, when extremely hot weather conditions lasting for 20–50 days occurred over South China (Wang et al., 2006); in 2015, which registered the hottest temperature recorded in western China at 47.7 °C (Su & Dong, 2019a, 2019b; Sun et al., 2016); in 2013 and 2017, when record-breaking heatwaves events occurred in eastern China (Sun et al., 2014a,b; Xia et al., 2016, 2018); and in 2022, which featured an unprecedented summer of extremely high temperatures (induced massive wildfires in Chongqing municipality) and severe drought in the Yangtze River basin in China (Lu et al., 2022). Furthermore, urban heatwaves have become increasingly concerning in individual cities and urban agglomerations throughout China (Chen et al., 2015; Huang et al., 2010; Jiang et al., 2019; Li et al., 2016, 2021; Liao et al., 2018). However, CDNG heatwaves have rarely been addressed in China, with only the publications by An and Zuo (2021), Chen and Zhai (2017), and Zhang et al. (2020) studying the characteristics of DYT, NGT, and CDNG heatwaves events in the Huai River Basin and China. Due to the serious threat posed by heatwaves, it is of great importance to understand and quantify the causes underlying their intensities (Kong et al., 2020), specifically CDNG heatwaves events, which are especially dangerous to human health (An & Zuo, 2021; Murage et al., 2017).

In recent years, Southwest China has encountered frequent heatwaves events. This has led many scholars to devote their studies to revealing the temporal and spatial changes (Chuan et al., 2022; Liao et al., 2022; Wang et al., 2015) of the heatwaves and their impact mechanisms (Deng et al., 2020; Huang et al., 2021; Liu et al., 2022) in Southwest China. However, the above-mentioned research has mainly focused on summer daytime or nighttime air temperature heatwaves, and the station classification method mainly based on absolute thresholds. Furthermore, urban heat island research describes the phenomenon in which air temperature and land surface temperature are obviously higher in urban areas than that in peripheral suburbs (Yin et al., 2018). This means that the urban heat island effects typically impact both air and land surface temperatures (Marzban, Sodoudi & Preusker, 2018). Air temperature is usually measured as the canopy layer heat island and the boundary layer heat island, while land surface temperature is typically derived from satellite-based remote sensing data (Yin et al., 2018). Air temperature urban heat islands generally exhibit greater spatial variability at night, while land surface temperature urban heat islands usually occur during the daytime (Zhou et al., 2011). As a high-temperature events, understanding the mechanisms influencing air temperatures and land surface temperatures during heatwaves is important in the development of urban adaptation strategies and creating eco-friendly and environmentally sustainable urban areas (He et al., 2020; Xiang et al., 2021). However, as we all acknowledge, there are no relevant studies that combine air and surface temperatures based on observation stations to reveal the characteristics of heatwaves changes in the Southwest China.

In this study, we conducted a case study using Southwest China to investigate the characteristics of DYT, NGT, and CDGN heatwaves. The novelty and scientific contribution of this research are mainly found in the following two aspects: from a methodology perspective, this study used high quality monitoring station data (Section 2.2) to establish a daily basis percentage threshold to dynamically calculate heatwaves based on relative (consider the difference of social and economic development) and absolute thresholds (fixed threshold) for urban, suburban, and rural stations using both air and surface temperatures. Secondly, for the first time, based on the air and land temperatures, the spatiotemporal variation of DYT, NGT, and CDNG heatwaves and the corresponding differences in meteorological elements and urbanization effects are revealed in Southwest China. This region provides an interesting case study which can act as a theoretical basis for better relating changes in heatwaves at urban stations with diverse terrain features and degrees urban expansion to the temporal dynamics of regional thermal environments. The objectives of this study include: (1) to investigate the historical spatiotemporal patterns of air and surface temperatures during heatwaves; (2) to explore DYT, NGT, and CDNG heatwaves and compare differences in air and surface temperatures among urban, suburban, and rural stations using different buffer zones based on relative and absolute dynamic threshold classifications; and (3) to evaluate the impacts of urban expansion on air and surface temperatures and DYT, NGT, and CDNG heatwaves. The resulting improved understanding provides urban policy makers and planners with a basic knowledge of the mechanisms by which urbanization affects heatwaves and provides a reference model to help basin, mountain, plateau, and karst cities (megacities) achieve sustainable cities and communities (Sustainable Development Goal 11) and improve urban climate risk management and climate resilience (Sustainable Development Goal 13).

## 2. Data and methodology

### 2.1. Study region

Southwest China includes mountains, plateaus, basins, karst topography, and other landforms, together they span three distinct regions representing extreme height differences from over 4000 m in the Tibetan Plateau to less than 500 m in the Sichuan Basin, and they are representative of the variability across Southwest China (Qin et al., 2010). The topography and geomorphology have led to the unique climate characteristics of Southwest China, thus making Southwest China a global biodiversity center, as well as an area that is most vulnerable to the threat of extreme climate events. Examples of the sensitivity are the continuous drought that occurred in Southwest China from autumn 2009 to spring 2010 (Li et al., 2019a), from spring to early summer 2019 in Yunnan province (Wang et al., 2021b), in the summer of 2014 (26 days with air temperature above 35 °C; maximum temperature of 39 °C lasted four days from August 5 to August 8), the years of 2016, 2018, 2020, and 2021 in Chongqing municipality, each with extreme air

temperatures reaching 39 °C or even 40.1 °C (Chongqing Meteorological Bureau, 2021), and the summer of 2022, which also has had high temperatures with the strongest comprehensive intensity since 1961 in Chongqing municipality, Sichuan Province. In particular, the daily maximum temperature in Chongqing municipality (Beibei, Jiangjin station) reached 44 °C (Xia et al., 2022). Moreover, high temperature and drought events often occur together, making Southwest China the only region where the drought severity and heatwaves days have both increased substantially, which could lead to increasing impacts on the environment and human society, as well as economic repercussions (Deng et al., 2020).

Southwest China (in this study, mainly the three provinces of Sichuan (SC), Yunnan (YN), and Guizhou (GZ), as well as the municipality of Chongqing (CQ)) is an important part of the Yangtze River Economic Belt and has important strategic significance in the macro pattern of China's economic development. In 2021, the population of the study area was 212 million, accounting for about 15% of the national population. The regional GDP was 12.68 trillion yuan, accounting for 11.08% of the national GDP (National Bureau of Statistics of the People's Republic of China, 2021). There are three major urban agglomerations in Southwest China, the Chengdu-Chongqing, Central Guizhou, and Central Yunnan urban agglomerations, which were approved by the National Development and Reform Commission in 2016, 2017, and 2020, respectively. Furthermore, in the capital cities of three provinces in Southwest China (Chengdu, Kunming, and Guiyang) and municipality directly under the Central Government of Chongqing, the urban built-up areas have grown rapidly in 2010–2020 (Chuan et al., 2022; Huang et al., 2021; Liao et al., 2022; Liu et al., 2022) and their rapid expansion has exacerbated the urban heat island effect and influenced heatwaves.

### 2.2. Data sources

Daily air (surface) maximum ($T_{max}$), minimum ($T_{min}$), and relative humidity data were provided by the National Meteorological Information Center of the China Meteorological Administration (http://data.cma.cn). The vapor pressure deficit and atmospheric water vapor pressure were calculated according to published methods (Luo & Lau, 2019). The dataset was subjected to quality control and homogeneity testing before being used. Because there were many missing measurements and errors in the surface temperature data prior to 1980, we focused on air and surface temperature data for the 1980–2019 period, which is also a period of rapid urbanization. Station migration was the main factor causing sudden changes in meteorological data, so the following conditions were adopted during station selection to guarantee the reliability of the data: (1) retain stations with migration distances less than 20 km and vertical height displacements within 100 m from 1980 to 2019, and the station should not have been relocated more than 2 times (station relocation was frequent before 1980, but less after); and (2) stations missing measurements more than three days per month are excluded. For those missing fewer than three days of measurements, data were filled in by applying the linear regression between elevation and data from the surrounding stations during 1980–2019. The above strict criteria resulted in the final inclusion of 332 air temperature stations and 297 surface temperature stations. Land use and cover data from eight years (i.e., 1980,1990, 1995, 2000, 2005, 2010, 2015, and 2018) with resolutions of 30 m were retrieved from the Resource and Environment Science and Data Center of China (http://www.resdc.cn/).

### 2.3. Methodology

#### 2.3.1. Dynamic classification of urban, suburban, and rural stations

The urban, suburban, and rural stations were classified dynamically based on the time-varying land use and cover maps available for eight different years (i.e., 1980, 1990, 1995, 2000, 2005, 2010, 2015, and 2018) following previous studies (Luo & Lau, 2021; Ren et al., 2015; Sun et al., 2016; Wang et al., 2021a). First, circular buffers with radiuses of 2 km, 5 km, 7 km, 10 km, and 15 km were constructed for each station and the proportions of built-up areas within the buffer areas were calculated. Note that each station can have different built-up areas for different subperiods because the built-up areas for each station were calculated based on the time-varying land use and cover maps data for each of the eight subperiods: 1981–1990, 1991–1995, 1996–2000, 2001–2005, 2010–2015, and 2016–2020, depending on the availability of land use and cover data. Previous studies (Liao et al., 2018; Luo & Lau, 2021; Ma et al., 2021; Wang et al., 2021a; Wu et al., 2020) have classified stations with 33.3%, 20%, 15%, or more built-up area in 2 km, 7 km, and 20 km buffers in a subperiod as urban stations; otherwise, they were categorized as rural (Liao et al., 2018; Sun et al., 2016). Furthermore, Ren et al. (2015) and Li et al. (2019b) further distinguished suburban stations as those that were less than 5 km from an urban polygon or as areas where the proportion covered by human settlement exceeded 33 or 22% in a buffer zone area of 12 $km^2$ or a radius of 11 km, respectively. Herein we used two methods to dynamically classify urban, suburban, and rural stations, i.e., the first method used absolute thresholds according to previous research (Li et al., 2019b) to define urban areas as those with built-up areas that exceeded 33%, 25%, 20%, 15%, and 10% in 2 km, 5 km, 7 km, 10 km, and 15 km buffer zones, suburban stations were those located within 5 km of urban areas with greater than 25% built-up areas, and other stations were rural stations. The second method used relative thresholds that considered the differences in social and economic development among Chongqing, Sichuan, Yunnan, and Guizhou provinces while calculating the built-up areas in five buffer zones (2 km, 5 km, 7 km, 10 km, and 15 km) separately in eight land use periods (1980, 1990, 1995, 2000, 2005, 2010, 2015, and 2018). In this method, if a station's built-up area exceeds the average value of the built-up areas of all stations within its province in that year, it is defined as an urban station, and a 5 km buffer zone is established around the urban areas, if a station occurs within the buffer around the urban polygon (land for large, medium, and small cities and built-up areas above counties and towns) and its built-up area exceeds the average built-up area value of all remaining stations (non-urban) in that year, it is regarded as a suburban station, the rest of the stations are defined as rural stations. For more detail please see supplementary material.

#### 2.3.2. Definitions of heatwave extremes

A day/night is considered hot when the maximum (minimum) air and surface temperature (i.e., $T_{max}$ and $T_{min}$) is higher than the historical 90th percentile for that specific calendar day. The adoption of daily percentiles avoids possible inhomogeneity in frequency and intensity series of temperature extremes (Wang et al., 2021a; Zhang et al., 2005). For each calendar day, the 90th percentile of maximum (minimum) air and surface temperature is calculated from multiyear sample measurements from 15 days samples surrounding this day (7 days on either side of the specific day, i.e., total samples $15 \times 40 = 600$ days) by ranking historical values from 1980 to 2019, three types hot events were defined as follows:

1.An independent hot day - an extreme hot day not followed by an extreme hot night ($T_{max} \geq$ 90th percentile and $T_{min} <$ 90th percentile);
2.An independent hot night - an extreme hot night not preceded by a hot day ($T_{min} \geq$ 90th percentile and $T_{max} <$ 90th percentile);
3.A compound hot event - a day where both $T_{max}$ and $T_{min}$ are extremely high ($T_{max} \geq$ 90th percentile and $T_{min} \geq$ 90th percentile; in the order of hot day preceding the hot night). Detailed information for these heat extremes is provided in Table 1.

#### 2.3.3. Identification of spatial expansion of heatwaves

Ren (2012) proposed an objective identification method for regional extreme events that considers their spatiotemporal continuity. Wang and Yan (2021) extended their concept to create an identification

**Table 1**
Details of heat extremes and variability.

| Heat extremes | Threshold | Units |
|---|---|---|
| Daytime hot day (DT) | $T_{max}$≥90th percentile and $T_{min}$ < 90thpercentile | 1 day |
| Nighttime hot day (NT) | $T_{min}$≥90percentile | 1 day |
| Compound daytime and nighttime hot day (CDN) | $T_{min}$ ≥90th percentile and $T_{max}$< 90thpercentile | 1 day |
| Compound daytime and nighttime heatwave (CDNH) | $T_{max}$ ≥90th percentile and $T_{min}$ ≥ 90thpercentile | ≥3 days |
| YDTN | Yearly number of daytime hot days | days |
| YNTN | Yearly number of nighttime hot days | days |
| YCDNN | Yearly number of compound daytime and nighttime hot days | days |
| YCDNHN | Yearly number of compound daytime and nighttime heatwaves | events |
| YCDNHP | Yearly sum of participating compound daytime and nighttime heatwave days | days |
| YCDNHM | The magnitude of compound daytime and nighttime heatwaves within a year | $°C^2$ |

approach for regional extreme events by combining it with an algorithm for density-based spatial clustering applications with noise (DBSCAN) (Ester et al., 1996) to objectively identify any clusters of hot stations, i.e., heat patches. Without any prior knowledge of the number of clusters or requirements for cluster form, the DBSCAN approach can find arbitrarily shaped station clusters and solitary stations. As a result, the number of station clusters can be objectively calculated, and any solitary stations can be immediately removed (Wang & Yan, 2021). Meanwhile, the DBSCAN clustering algorithm can be improved by using the ratio, rather than the absolute density, of surrounding hot stations. Therefore, we should focus more on regional concurrent heatwaves events. The procedure for identifying regional concurrent heatwaves events is as follows:

(1)The metrological stations with $T_{max}$ and $T_{min}$ based on air and surface temperature for concurrent daytime and nighttime heatwaves over the threshold are labelled 1, the others are labelled 0 as isolated hot stations.
(2)BDSCAN is adopted to cluster the 0 and 1 stations and extract regional signals of compound heatwave events from 1980 to 2019.
(3)Heat patches occurring on two consecutive days are identified as propagating hot events if they overlap spatially by more than 20% (i.e., the overlapping ratio threshold: V0); otherwise, we classify the prior day's heat patch as a temporary discontinuous heat patch and it is ignored in further analyses. If a heat patch on the current day overlaps with numerous heat patches from the previous day it is considered a combined propagating hot event.
(4)A propagating heatwaves as classified as a single regional event if it lasts at least three days, increasing the event count by 1; otherwise, it is treated as a disrupted heatwave and is ignored in further analyses. We consider an event to have ended when the heat patch of a single regional heatwave on the day in question does not overlap with any heat patches on the following day by more than 20%. For more detailed information please see Table 2 and Wang and Yan (2021).

#### 2.3.4. Other methods

Sen's slope estimator and the Mann-Kendall trend test method were used to determine slope magnitudes and trends (Mann, 1945; Pettitt, 1979; Sen, 1968; Theil, 1950). Heatwaves indices (Table 1) were interpolated using a digital elevation model into a raster with 1-km resolution using an ensemble of six algorithms (i.e., boosted regression tree, neural network, generalized additive model, multivariate adaptive regression spline, support vector machine, and random forest). During model tuning, each algorithm is systematically weighted from 0 to 1 and the fit of the ensembled model is evaluated. The best performing model

**Table 2**
Values of the parameters of the DBSCAN clustering in Southwest China.

| Parameter name | Code | Meaning | Value |
|---|---|---|---|
| Daily air and surface temperature threshold of single station | T | Threshold of daily air and surface temperature anomaly stations. | Daily maximum and minimum AT and ST |
| Threshold for the daily index | Tt | Abnormality occurs at individual stations only when air temperature and surface temperature is beyond Tt. | The 90% percentile of maximum and minimum air and surface temperature |
| Threshold for the neighbor station distance | d0 | Search the maximum nearest distance between any two stations within the scope of a specific surrounding region (d0) and consider them as neighbors, using the geographic position of the current hot station as the center of a circle. | 140 km (refer to Zhou et al., 2021a) |
| Threshold for the neighboring abnormality ratio | R0 | The current hot station is designated as a clustered hot station belonging to cluster R0 if the ratio of surrounding hot stations (n) to all neighboring stations (N; includes both hot and normal stations) for the current hot station is greater than the provided threshold (R0). | 0.4 |
| Threshold for number of abnormality stations in a heat patches | M0 | a hot station in a cluster with at least $N \times$ R0 nearby hot stations in its immediate vicinity, and an isolated hot station, i.e., a hot station that is not part of any cluster. Assign numbers to groups of at least10 hot stations as regional heat patches. | 10 |
| Heat patches on two consecutive days overlap ratio | V0 | If two heat patches on two consecutive days overlapping ratio than 20% (repeated experiments found that the overlap ratio of 20% was the highest in Southwest China), consider them as a propagating hot event; otherwise, heat patch on the previous day as a temporally discontinuous heat patch that is not considered in subsequent analysis | 0.2 |

is determined through $k$-fold cross validation ($k = 10$) and the model with the lowest residual sum of squares of the test data is selected. However, if the $R^2$ value of final correction was greater than the $R^2$ value of the ensemble, the final correction was discarded (the $R^2$ values>0.8 for YDTN, YNTN,YCDNN,YCDNHN,YCDNHP, and YCDNHM) (Fig. 1).

## 3. Results

### 3.1. Spatial-temporal characteristics of heatwaves events

Fig. 2 shows the temporal changes in heatwaves events according to air temperature from 1980 to 2019. The highest average heatwaves values occurred in 2010, 2013, and 2015 for YCDNN, in 2010, 2011, and 2015 for YCDNHN and YCDNHP, and in 2009–2011 for YCDNHM.

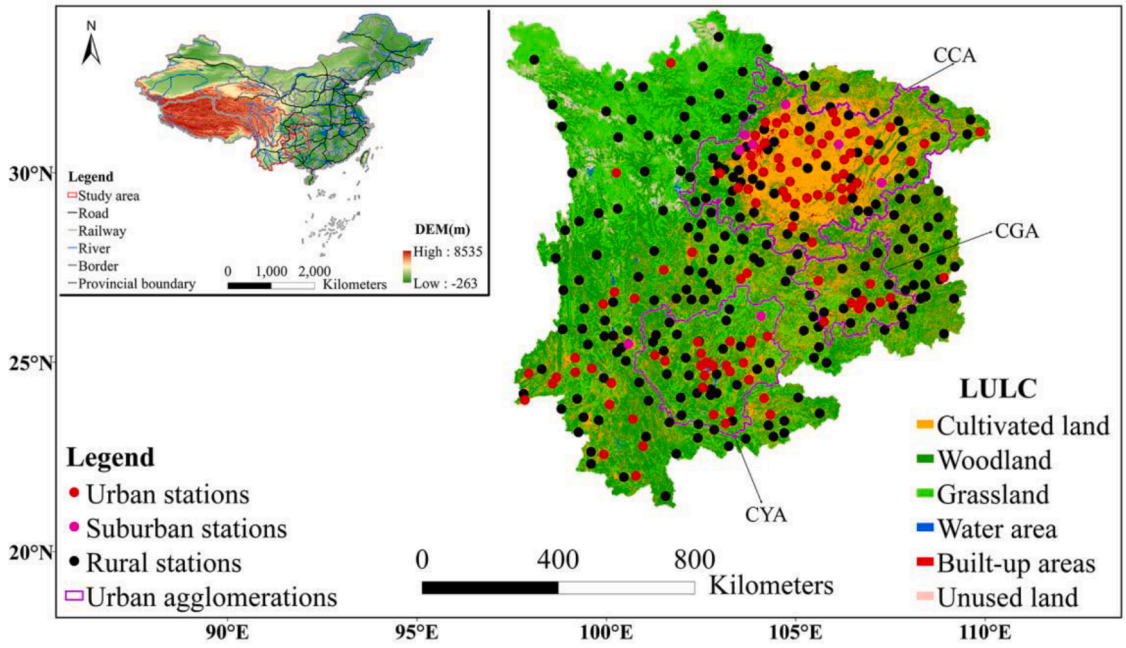


**Fig. 1.** Study area location, including rivers, roads, and urban agglomerations, as well as urban, suburban, and rural stations based on 2018 land use and land cover (LULC) within in 2 km buffer areas around stations (CCA: Chengdu-Chongqing agglomerations, CGA: Central Guizhou agglomerations, Central Yunnan agglomerations).

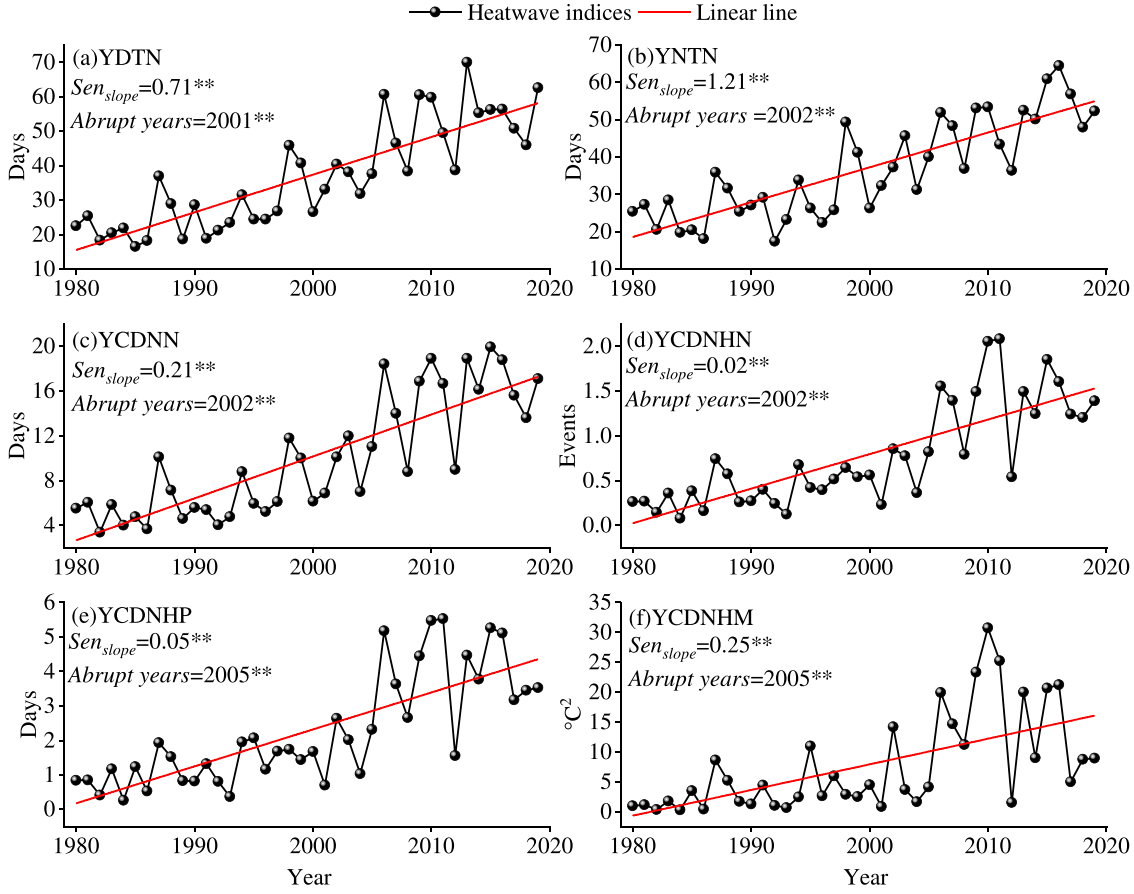


**Fig. 2.** Temporal characteristics of heatwaves indices based on air temperature during 1980–2020.

Significant ($p<0.05$) change trends were observed for all HW indices, the slopes of YDTN, YNTN, YCDNN, YCDNHN, YCDNHP, and YCDNM were 0.71 days/year, 1.21 days/year, 0.21 days/year, 0.02 events/year, 0.05 days/year, and 0.25 °C$^2$/year, respectively. Abrupt change years included 2001, 2002, and 2005 in which heatwaves became notably more severe in Southwest China. The annual YDTN from 34 (minimum) to 35.6 (maximum) days and decreased from southwest to northwest (Fig. 3a) for average 1980–2019, and 94.88% of stations had significant increases with only one station exhibiting a significant decrease; annual YNTN from 35.8 (minimum) in to 37.7 days for average 1980–2019 (Fig. 3b), high value areas were mainly concentrated in the south of Southwest China, and 89.76% of stations exhibited significant increases, with two stations showing significant decreases; annual YCDNN from 3.3 (minimum) in to 16.6 (maximum) days for average 1980–2019 (Fig. 3c), the high value areas were mainly distributed in the eastern part of SC and GZ and western CQ, and 93.98% stations showed significant increases, with one station decreasing significantly. Over the study period, the YCDNHN, YCDNHP, and YCDNHM from 0.04 to 1.6 events, 0 (minimum) to 27.4 (maximum) days, and 0.2 (minimum) to 4.7 (maximum) °C$^2$, respectively, with spatial patterns similar to that of YCDNN; of the 332 stations, 31% (104) of stations for YCDNHN, 36.7% (128) of stations for YCDNHP, and 38.6% (141) of stations for YCDNHM showed significant increases, with all other stations showing no significant change trends.

As shown in Fig. 4, the slopes of YDTN, YNTN, YCDNN, YCDNHN, YCDNHP, and YCDNM for ST all showed significant increases, at 1.06 days/year, 0.92 days/year, 0.35 days/year, 0.03 events/year, 0.09 days/year, and 0.29 °C$^2$/year, respectively, and years showing abrupt changes were 1998, 2002, and 2005. The average values of spatial patterns of the 6 heatwaves indices were similar to AT, whereas the slopes of the YDTN, YNTN, and YCDNN change trends of stations were obviously different, and YCDNHN, YCDNHP, and YCDNM significantly increased by 3.03%, 5.38%, and 6.16%, respectively, but showed no significant change at any other station (Fig. 5).

### 3.2. Increasing daytime, nighttime, and compound heatwaves based on absolute thresholds of air and surface temperatures in Southwest China

#### 3.2.1. Correlations between air and ground temperatures with urban expansion rate

For each station in the research region we created circular buffers with radiuses of 2, 5, 7, 10, and 15 km. Then, inside each circular buffer area, centered on a specific station, Spearman's correlation coefficients were used to examine the relationships between the average air temperature (332 stations) and surface temperature (297 stations) from 1980 to 2018 and the urban expansion rate. The correlations increased in strength with increasing radius for average and minimum air temperature, but decreased for maximum air temperature, whereas for surface temperature the correlations were insignificant except for average surface temperature with a 2 km radius and maximum ST with a 7 km radius. Therefore, in the following analysis, we dynamically extracted five buffer areas for urban, suburban, and rural stations according to the relative and absolute threshold station classification method. Fig. 6

Fig. 7 displays the dynamic classifications of urban, suburban, and rural stations in Southwest China based on time-varying land use and cover maps. Fig. 7a shows urban land use at four typical stations (Wenjiang, Shapingba, Guiyang, and Kunming) with 2, 5, 7, 10, and 15 km buffer areas where there were very obvious urban and other construction land expansion trends. According to the station classifications there were 13 (1, 317) urban (suburban, rural) stations using 2 km buffer areas in 1980, whereas there were 103 (9, 219) urban (suburban, rural) stations using 2 km buffer areas in 2018. A total of 98 rural stations were transformed into urban and suburban stations from 1980 to 2018.

#### 3.2.2. Temporal changes in heatwave indices based on air and surface temperatures

Fig. 8 demonstrates the long-term trends of all heatwaves indices over the period of 1980–2019 in Southwest China. All averaged heatwaves indices showed significant increasing trends in urban, suburban, and rural areas when using 2, 5, 7, 10, and 15 km buffer areas for air temperature, and the increases became steeper after 2005. Interestingly, the average values for all heatwaves indices (Fig. 10) of suburban stations with 5 km buffer zones were much higher than with other buffer zones when using air temperature (for YDTN and YNTN, the average values were ordered urban>rural>suburban with 2, 7, 10, and 15 km buffers). With regards to change trends, rural areas increased more than urban and suburban areas with 2, 5, 7, 10, and 15 km buffers for YDTN (except urban areas increased more than rural with 10 and 15 km buffers and suburban areas increased more than rural with 2 km buffers), the trends of urban and suburban areas were greater than rural for all buffer

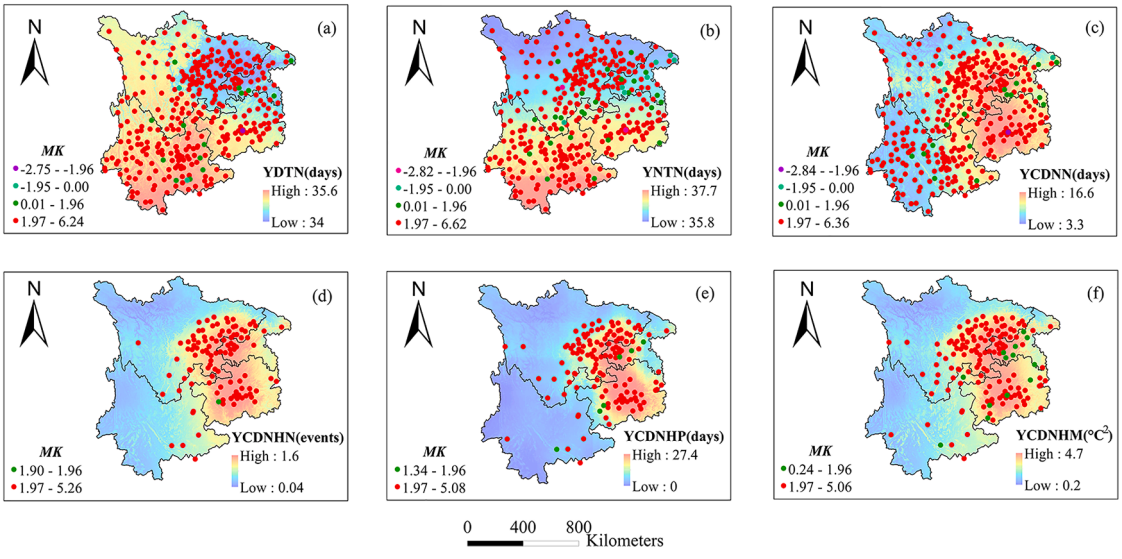


**Fig. 3.** Spatial characteristics of heatwaves indices based on air temperature for average 1980–2019.

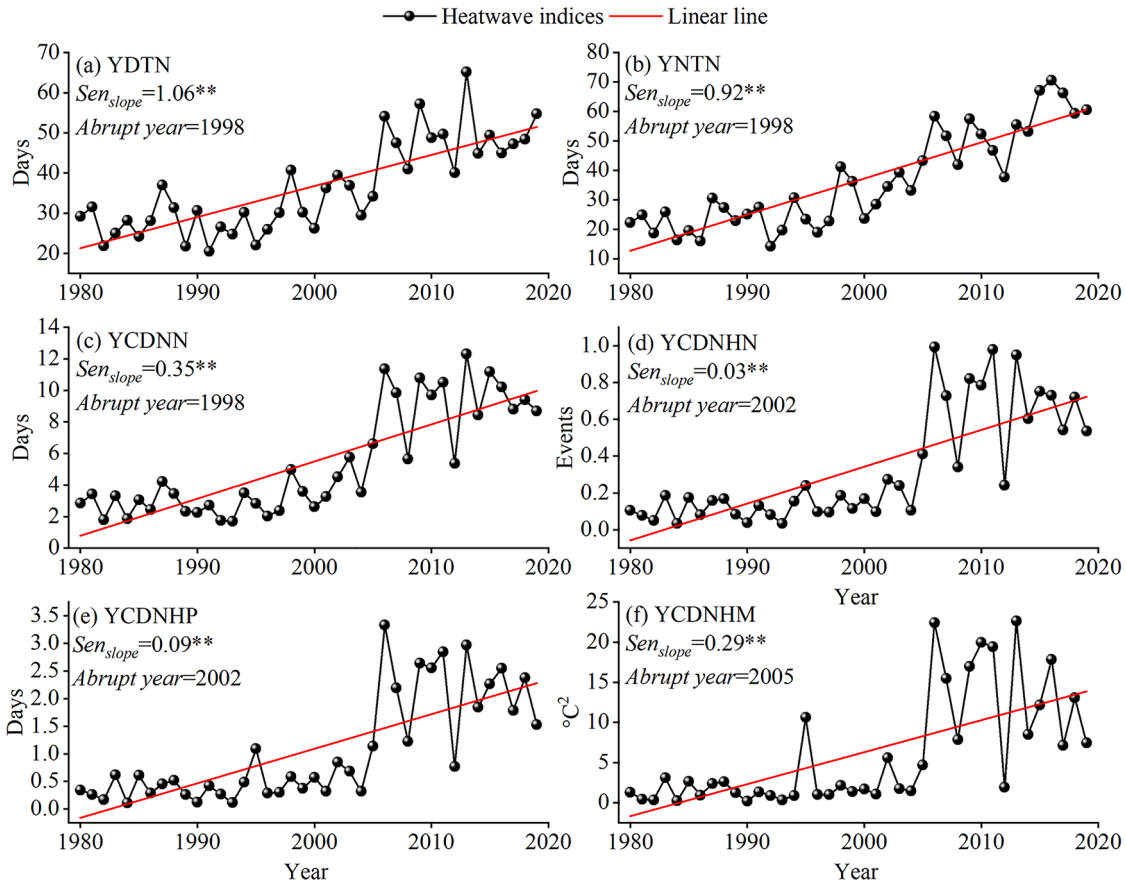


**Fig. 4.** Temporal characteristics of heatwaves indices based on surface temperature during 1980–2019.

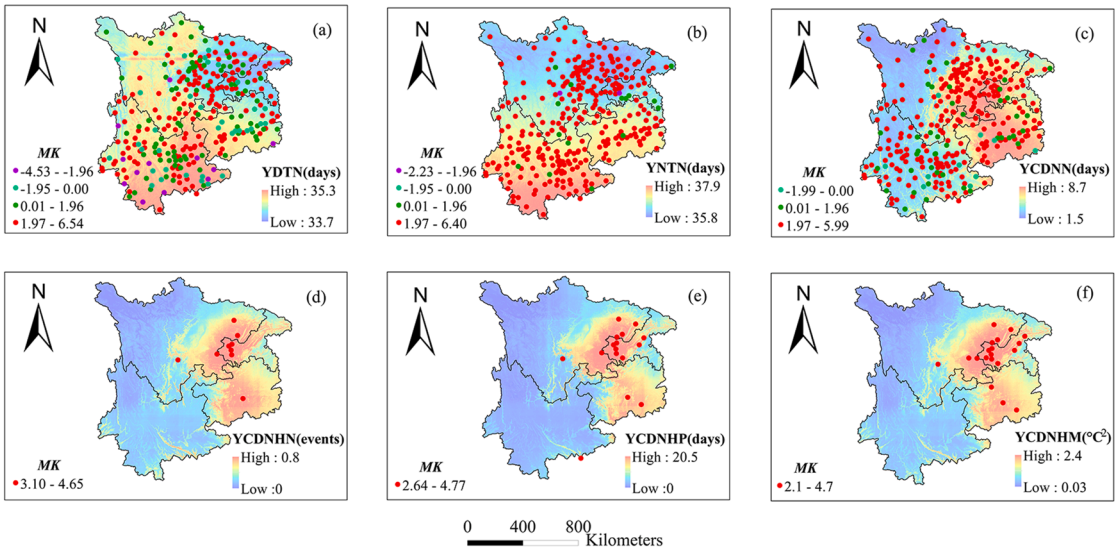


**Fig. 5.** Spatial characteristics of heatwaves indices based on surface temperature for average 1980–2019.

areas for YNTN (except in 7 km), YCDNN (except rural areas increased more than urban with 5 and 7 km buffers and rural areas increased more than suburban with 5, 7, 10, and 15 km buffers), and YCDNHP (except rural areas increased more than urban with 7 km buffers), whereas there was little difference in the change trends of YCDNHN for urban, suburban (except that suburban areas increased more than rural with 5 km buffers), and rural based on air temperature. Furthermore, similar to air temperature, all heatwaves indices based on ST increased obviously after 2005 (Fig. 9) and the average value (Fig. 10) of suburban heatwaves indices with 5 km buffers was much higher than when using other buffer zones for surface temperature (for YCDNN and YCDNHM, the average values were ordered suburban>urban>rural). However, the change trends of all heatwaves indices were obviously different when using air temperature. The trends of urban and suburban areas were

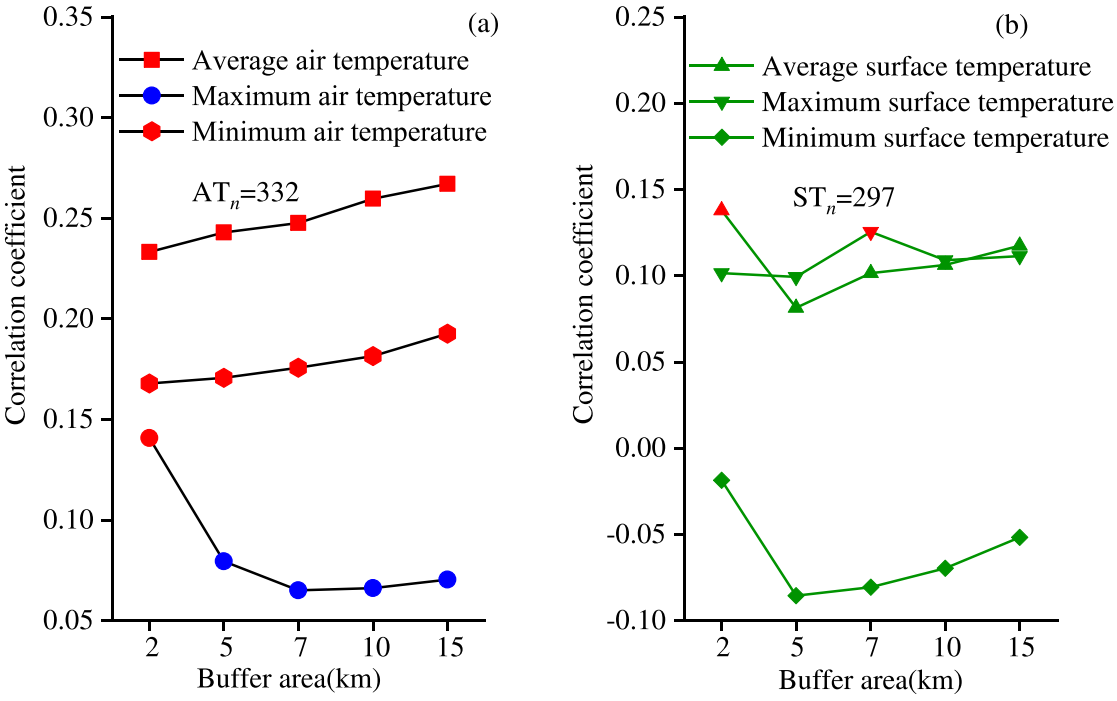


**Fig. 6.** Spearman's correlation coefficients between the air (a) and surface (b) temperatures (average, maximum, and minimum) and the urban expansion rate in the different buffered areas surrounding stations (red dots indicate a $p < 0.05$ significance level) from 1980 to 2018.

greater than rural for all buffer areas for YNTN (except in 7 km), YCDNN (except rural areas increased more than urban with 5 and 7 km buffers and rural areas increased more than suburban with 5, 7, 10, and 15 km buffers), and YCDNHP (except rural areas increased more than urban with 7 km buffers), whereas there was little difference in the change trends of YCDNHN for urban, suburban (except that suburban areas increased more than rural with 5 km buffers), and rural based on air temperature. For YCDNHN, the change trend was similar to the air temperature change trend, with small differences among urban, suburban, and rural areas with different buffer areas.

### *3.3. Increasing daytime, nighttime, and compound heatwaves for air and surface temperatures based on relative thresholds in Southwest China*

#### *3.3.1. Numbers of urban, suburban, and rural stations in each subperiod*

In 1980, the average built-up areas in the CQ/SC/YN/GZ areas were 9.8%/8.3%/8.5%/10.8%, 4.3%/3.9%/4.3%/3.7%, 3.0%/3.0%/3.1%/2.4%, 2.0%/2.3%/2.1%/1.7%, and 1.4%/1.8%/1.4%/0.9% within buffer areas of 2, 5, 7, 10, and 15 km around stations, respectively. Whereas in 2018, the average built-up areas in the CQ/SC/YN/GZ areas were 35.4%/27.1%/27.5%/27.9%, 21.6%/13.0%/14.4%/11.7%, 15.6%/9.5%/9.7%/8.1%, 11.1%/6.9%/6.2%/5.8%, and 7.3%/5.0%/3.9%/3.3% within buffer areas of 2, 5, 7, 10, and 15 km around stations, respectively. Due to rapid urbanization, built-up areas around stations increased sharply from 1980 to 2018. However, while the built-up areas of different buffer zones increased dramatically from 1980 to 2018, according to the relative threshold, the number of stations changing from rural to suburban and from rural or suburban to urban changed little within different buffer zones (Fig. 11b, c).

#### *3.3.2. Temporal changes in heatwaves based on air and surface temperatures*

Figs. 12 and 13 show the temporal characteristics of heatwaves indices based on air temperature for different buffer areas. As shown in Figs. 12a–f and 13a–f, the annual means of heatwaves indices changed obviously after 2005 for different buffer areas in the three provinces and municipality. There was little difference between the annual averages of YDTN and YNTN in the three provinces and municipality for urban, suburban, and rural stations with different buffer areas (Fig. 14). However, the YCDNN, YCDNHN, YCDNHP, and YCDNHM in urban and suburban areas were greater than rural areas in all three provinces and municipality (except in YN, where the rural and suburban areas were greater than urban areas for YCDNN, YCDNHN, YCDNHP, and YCDNHM, and in GZ, where rural areas were greater than suburban areas for YCDNN) with different buffer areas. For change trends, all heatwaves indices showed significant increasing trends in the three provinces and municipality, with the amplitudes of the increases generally ordered urban ≥ suburban>rural for the six heatwaves indices in different buffer areas in CQ, SC, and YN (except for YNTN in SC which was ordered urban>rural>suburban, and for YCDNHN, YCDNHP, and YCDNHM in YN which were ordered suburban>rural>urban) and mainly ordered suburban>rural>urban for YDTN, YNTN, and YCDNN, and suburban>urban>rural for YCDNN and YCDNHP in GZ for the different buffer areas.

The annual average heatwaves index values and change trends (significant increases in all six heatwaves indices in the three provinces and municipality) based on surface temperature were similar to those based on air temperature with different buffer areas for urban, suburban, and rural areas. Furthermore, the amplitudes of significant increasing trends for YDTN were generally ordered rural->suburban>urban in CQ, suburban>rural>urban in SC, urban->rural>suburban in YN, and rural>suburban>urban in GZ for different buffer areas. For YNTN, they were mainly ordered urban->rural>suburban in CQ and YN, rural>urban>suburban in SC, and rural>suburban>urban in GZ. For YCDNN, the orders were urban->suburban>rural in CQ, SC, and YN (except that rural>suburban for 2, 5, and 7 km buffers) and rural>suburban>urban in GZ. For YCDHNH, the orders were urban>suburban ≥ rural in CQ, urban ≥ suburban>rural in SC, rural>suburban>urban in YN, and suburban>rural>urban in GZ (except for the 2 and 5 km buffers). For YCDNHP, the orders were urban>suburban>rural in CQ and SC, rural->suburban>urban in YN, and suburban>rural ≥ urban in GZ (except in

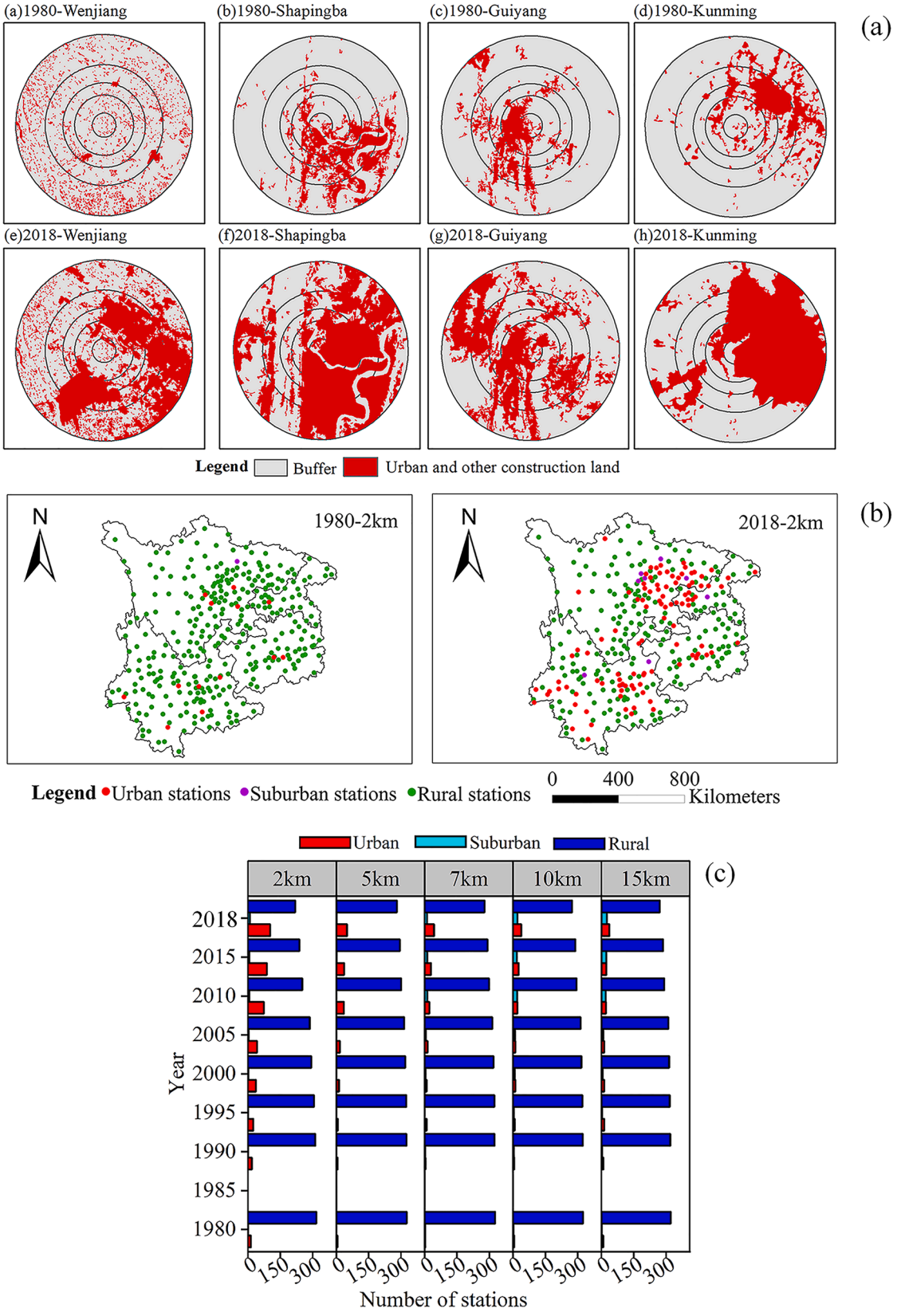


**Fig. 7.** Dynamic classifications of urban, suburban, and rural stations in Southwest China. (a) Urban land use of four typical stations (Wenjiang, Shapingba, Guiyang, and Kunming) using 2, 5, 7, 10, and 15 km buffer areas. (b) Urban, suburban, and rural stations using 2 km buffer areas in 1980 and 2018. (c) Dynamic changes in urban, suburban, and rural station types using 2, 5, 7, 10, and 15 km buffer areas in 1980–2018.

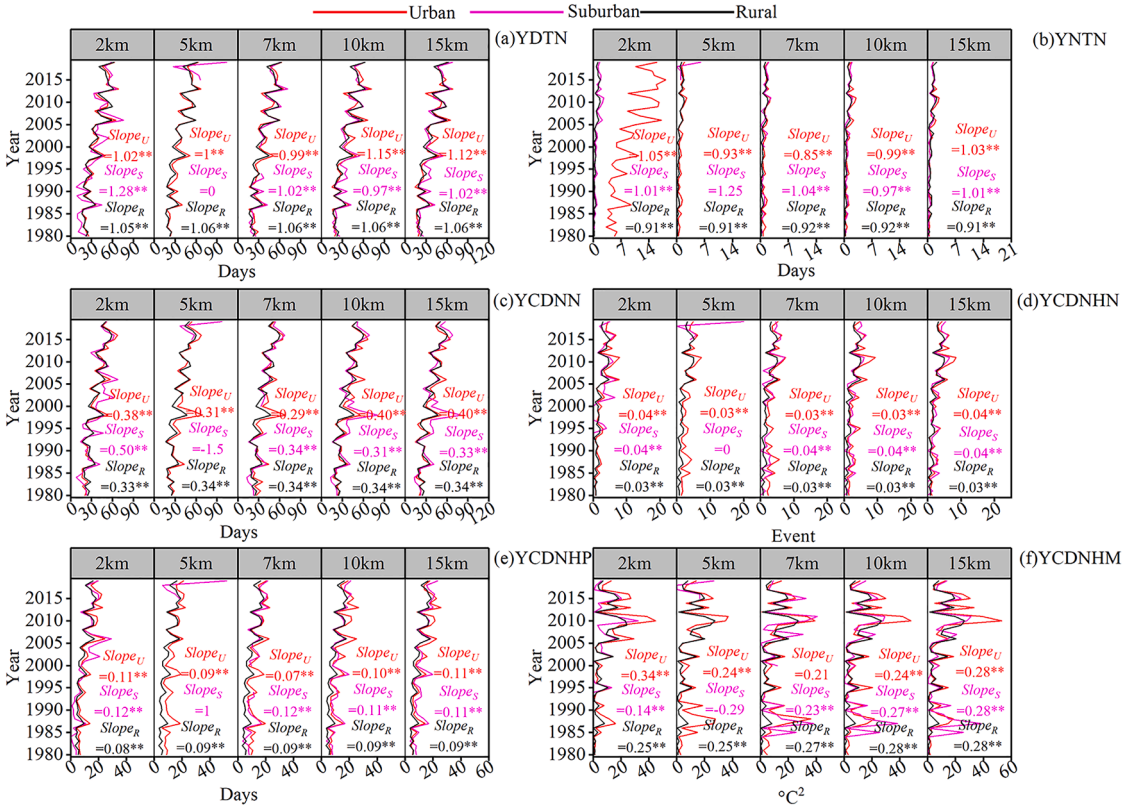


**Fig. 8.** Temporal characteristics of heatwave indices with different buffer areas based on air temperature.

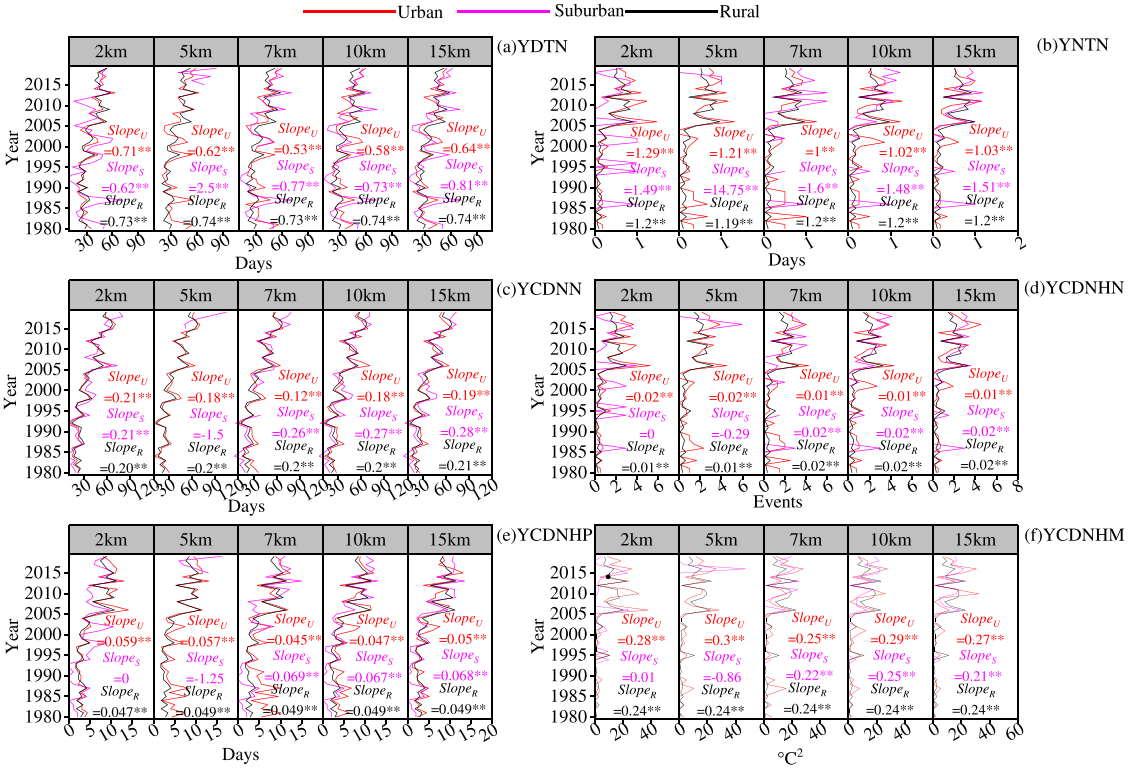


**Fig. 9.** Temporal characteristics of heatwaves indices with different buffer areas based on surface temperature.

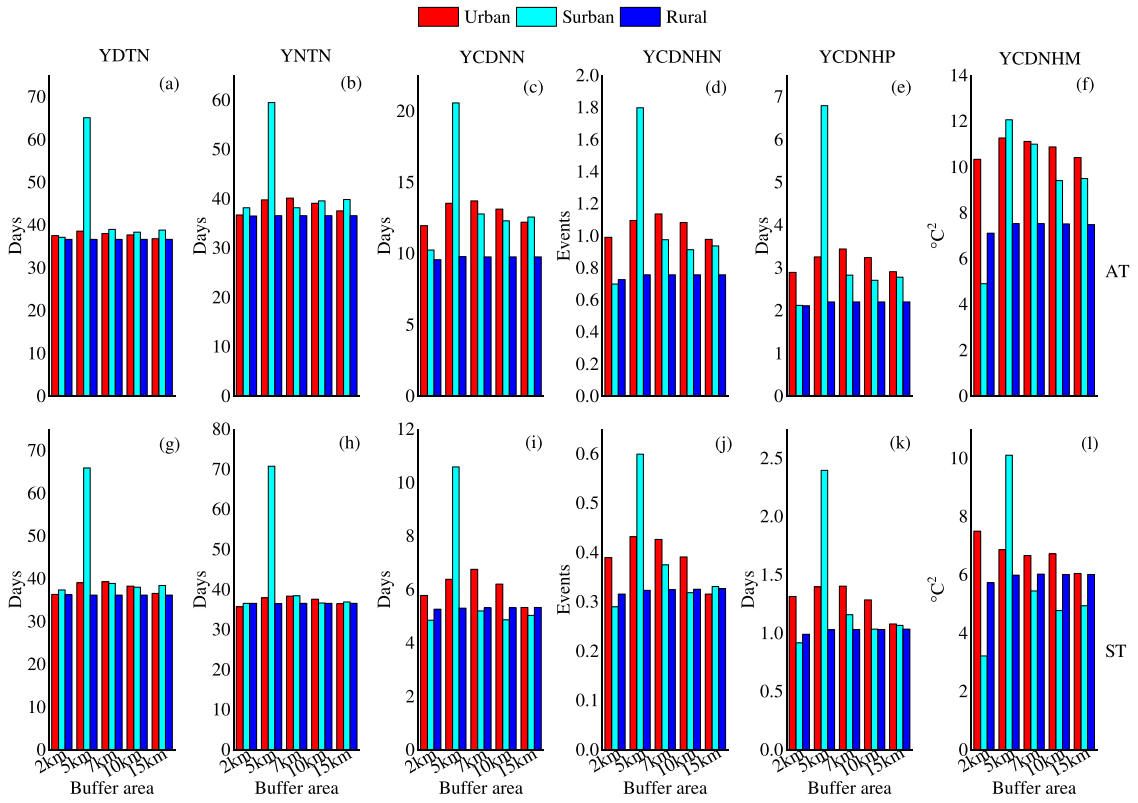


**Fig. 10.** Average value of heatwaves indices for urban, suburban, and rural areas with different buffer areas based on air and surface temperatures.

2 and 5 km). For YCDNHM, they were ordered urban>suburban ≥ rural in CQ, suburban>urban>rural in SC (except for 2 and 5 km buffers) and YZ (except for the 2 km buffer), and suburban>rural>urban in GZ (except for the 2 km buffer) (Figs. 15–17).

### 3.4. Spatially persistent compound heatwaves (YCDNHM) based on air and surface temperature

Using the DBSCN method, we extracted 20 regional heatwaves events based on the YCDNHM (YCDNHM takes into account both amplitude (intensity per unit time) and length of concurrent heatwaves) index based on air temperature, of which the three longest duration heatwaves events (see Table 3) were September 5–15, 2009 (duration: 10 days, average: 3.5 $°C^2$, maximum: 3.5 $°C^2$), August 17–26, 2016 (duration: 9 days, average: 2.51 $°C^2$, maximum: 5.87 $°C^2$), and January 30–February 7, 2013 (duration: 10 days, average: 10.35 $°C^2$, maximum: 17.18 $°C^2$). In terms of intensity, the heatwaves event in 2013 was the most prominent. Furthermore, Fig. 18 shows a typical day of the longest regional heatwaves event of temporal and spatial evolution for magnitude of CDNG (units: $°C^2$) at clustered hot stations for the most extreme regional heatwaves event of 1980–2019 in Southwest China, which lasted 5–15 September 2009 based on air temperature. The heatwaves event initially occurred along the western edge of Sichuan Basin, gradually propagating to the middle and eastern parts of SC, it remained in the central and eastern parts of SC, western part of CQ, and the northeast of YN until September 11, at which point it propagated to the central and western part of YN and dissipated (Fig. 19).

Furthermore, Table 4 provides information on three regional heatwaves events based on surface temperature that occurred in 2009, 2010, and 2016. The spatial propagation patterns manifested in these three years were mainly in the east of SC, the west of CQ, and the northeast of YN, respectively, and then disappeared in the east of YN.

### 3.5. Possible impact underlying meteorological factors and urban expansion

It can be seen from Fig. 20a, b that the air and surface temperature heatwaves indices were significantly positively correlated with vapor pressure deficit and negatively correlated with relative humidity. We also found that the heatwaves indices YCDNN, YCDNHN, YCDNHP, and YCDNHM had significant positive correlations with the maximum air and surface temperature, and the correlation coefficient was strongest among the three temperature indices. Therefore, it can be inferred that the heatwaves in Southwest China may be best monitored using maximum temperatures. Meanwhile, it can be seen from Fig. 21 that, according to the dynamic classify method of absolute and relative thresholds, vapor pressure deficit had a significant increasing trend while relative humidity had a significant decreasing trend during the study period. However, there was a faster increase in vapor pressure deficit in urban and suburban areas compared to rural areas and a faster decrease in relative humidity in rural areas when using different buffer areas in SWC (absolute thresholds), and CQ and SC (relative thresholds), while rural areas had a faster increase in vapor pressure deficit than urban areas and a faster decrease in relative humidity than urban and suburban areas when using different buffer areas in YN and GZ (relative thresholds), except in suburban area in GZ. Furthermore, Fig. 22 shows that urbanization positively contributed to air and surface temperature heatwaves when using different buffer zone areas in CQ and SC, whereas urbanization had a negative effect on heatwaves in YN, GZ, and SWC when buffer zones with 2, 5, 7, 10, and 15 km radiuses were used. This showed that different classification methods (absolute and relative thresholds) obviously affect the calculated contributions of urbanization to heatwaves in Southwest China.

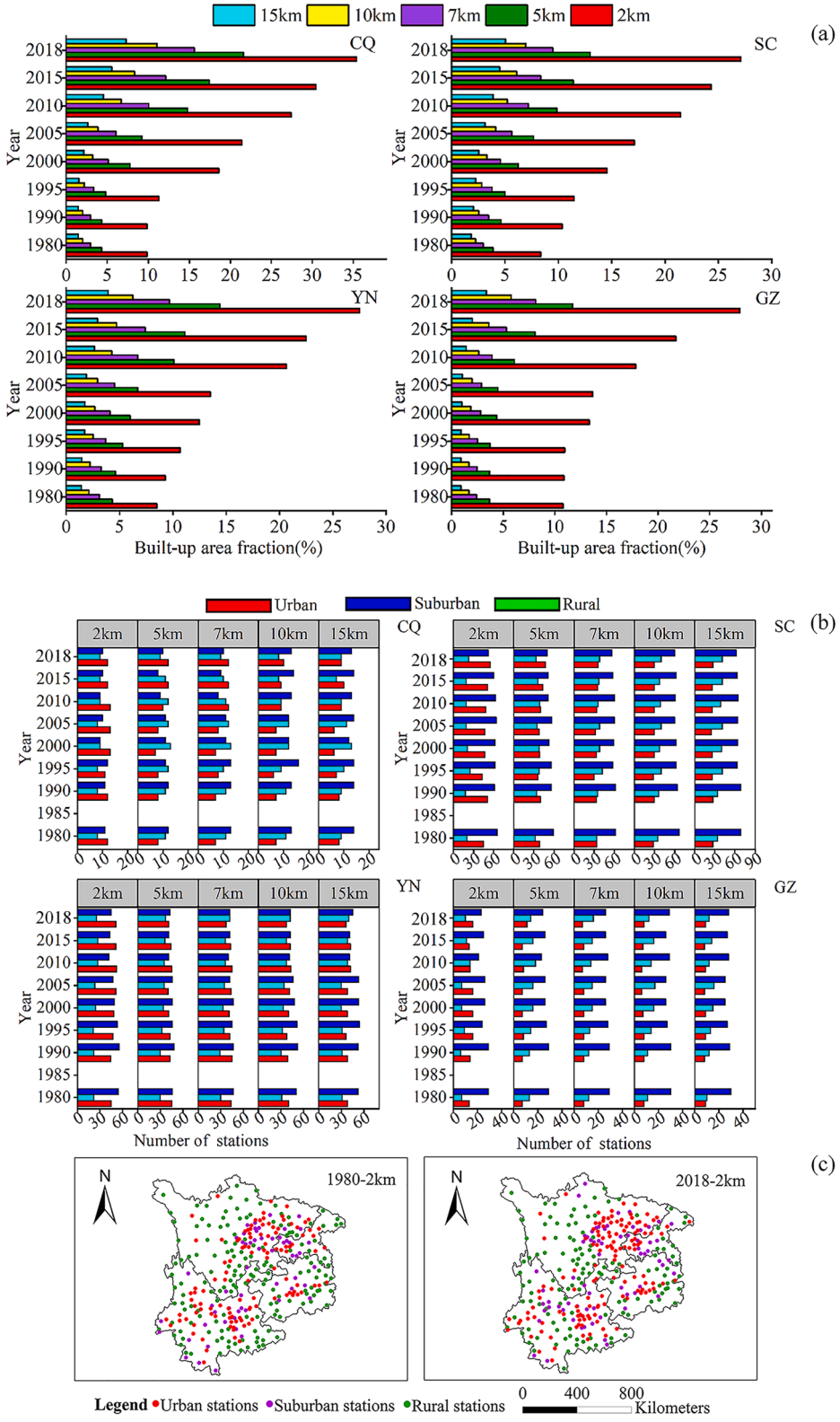


**Fig. 11.** Dynamic classifications of urban and rural stations in Southwest China. (a) Changes in built-up fraction from 1980 to 2018 for different buffer areas; (b) changes in numbers of urban, suburban, and rural stations from 1980 to 2018; (c) spatial distributions of urban, suburban, and rural stations in 1980 and in 2018 using 2 km buffer areas.

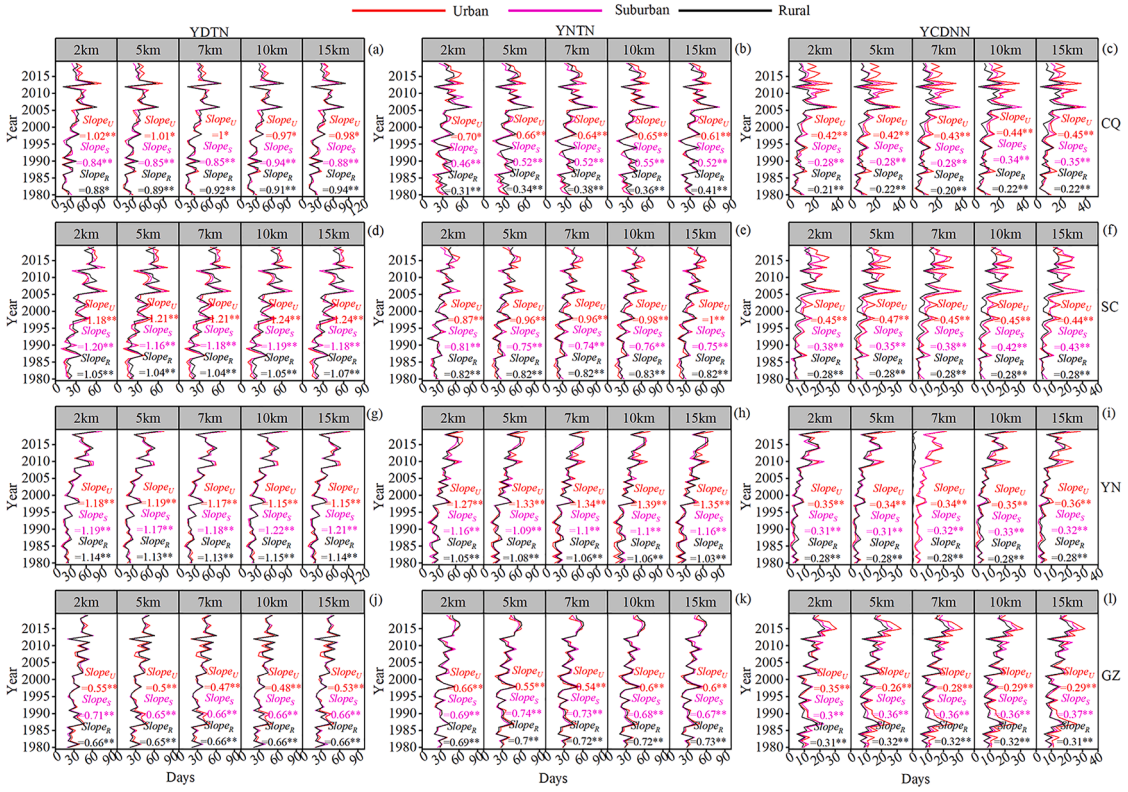


**Fig. 12.** Dynamic temporal characteristics of heatwave indices (YDTN, YNTN, and YCDNN) with different buffer areas based on air temperature.

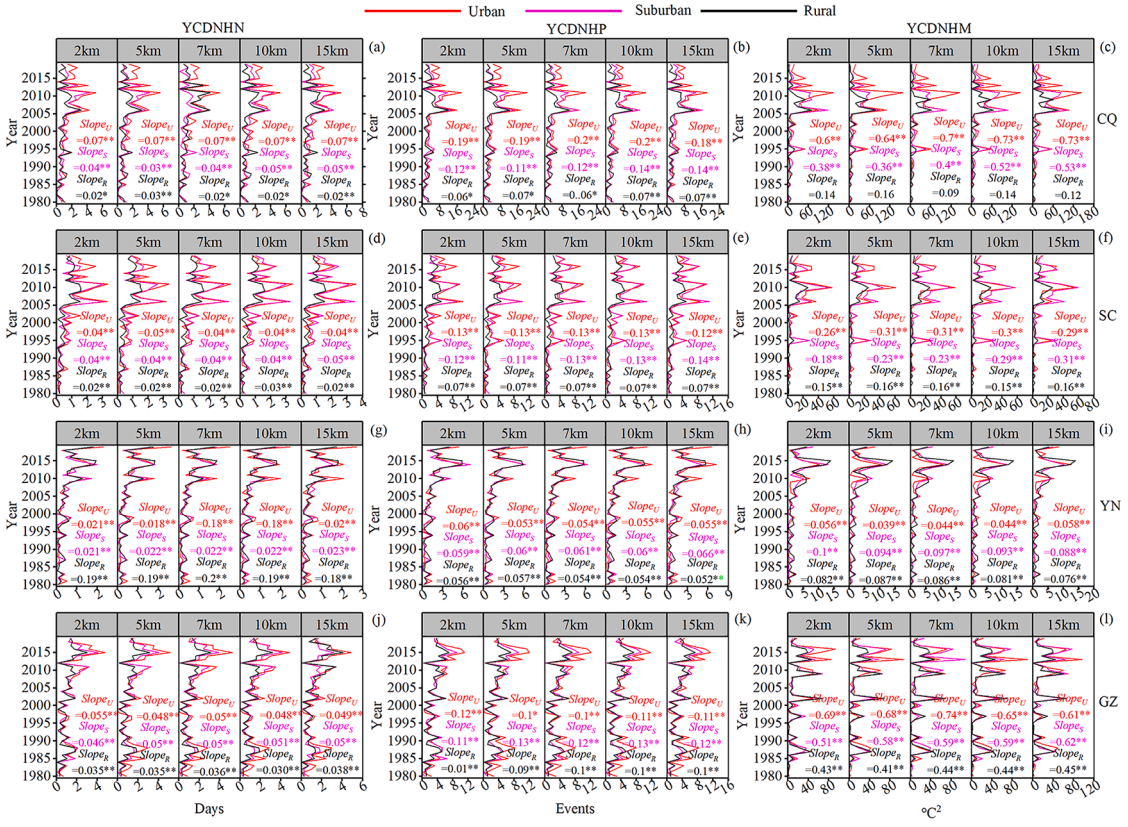


**Fig. 13.** Dynamic temporal characteristics of heatwave indices (YCDNHN, YCDNHP, and YCDNHM) for different buffer areas based on air temperature.

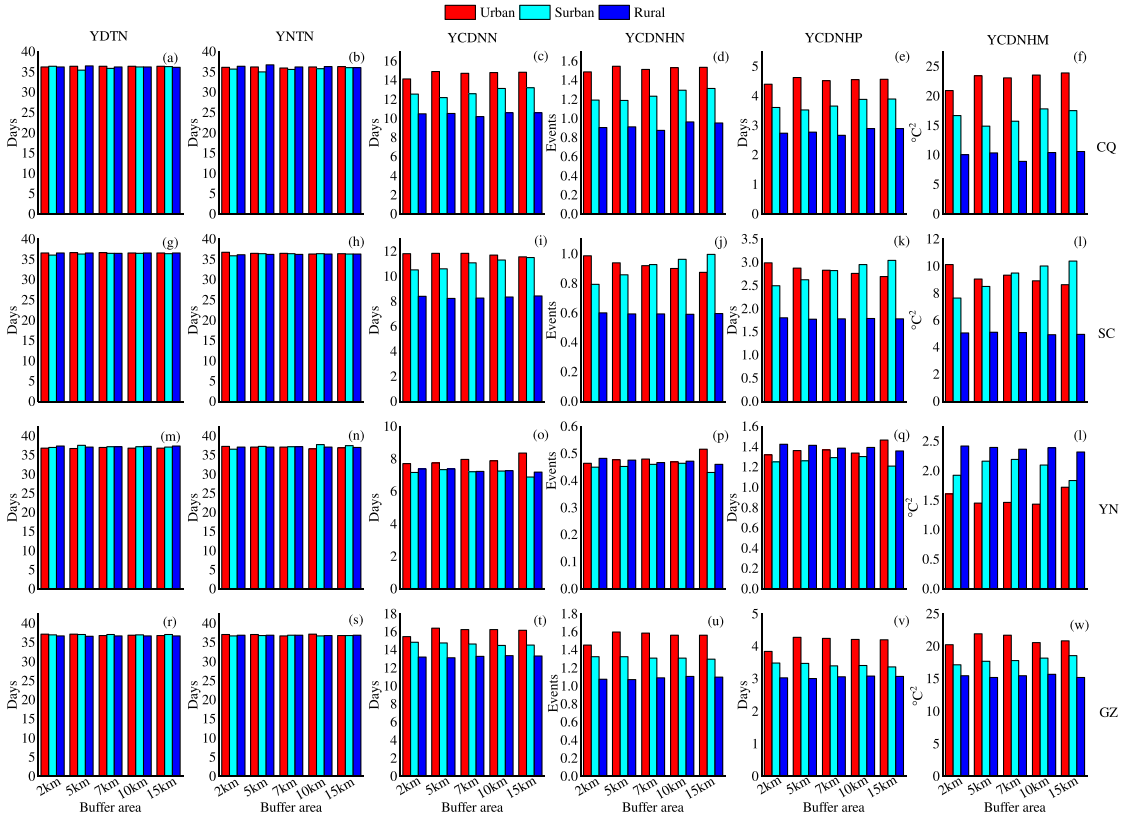


**Fig. 14.** Average heatwaves indices for urban, suburban, and rural areas using different buffer areas based on air temperature.

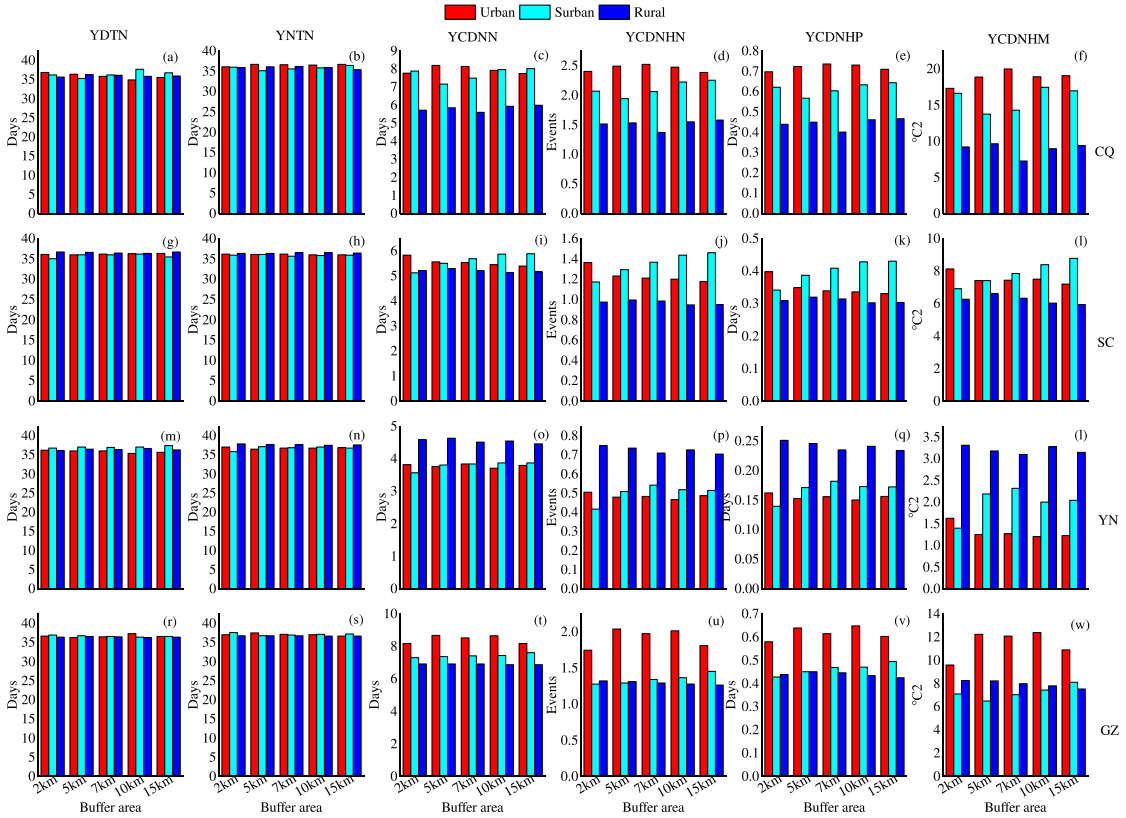


**Fig. 15.** Average heatwaves indices for urban, suburban, and rural areas using different buffer areas based on surface temperature.

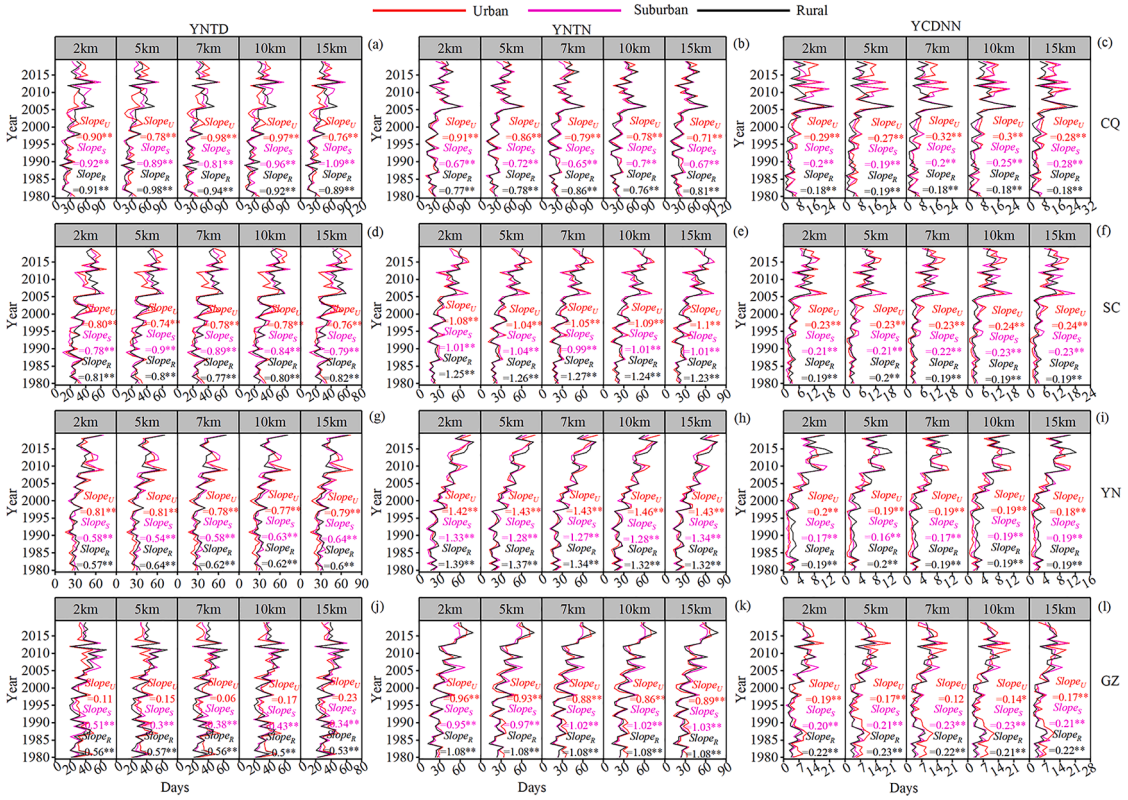


**Fig. 16.** Dynamic temporal characteristics of heatwaves indices (YDTN, YNTN, and YCDNN) for different buffer areas based on surface temperature.

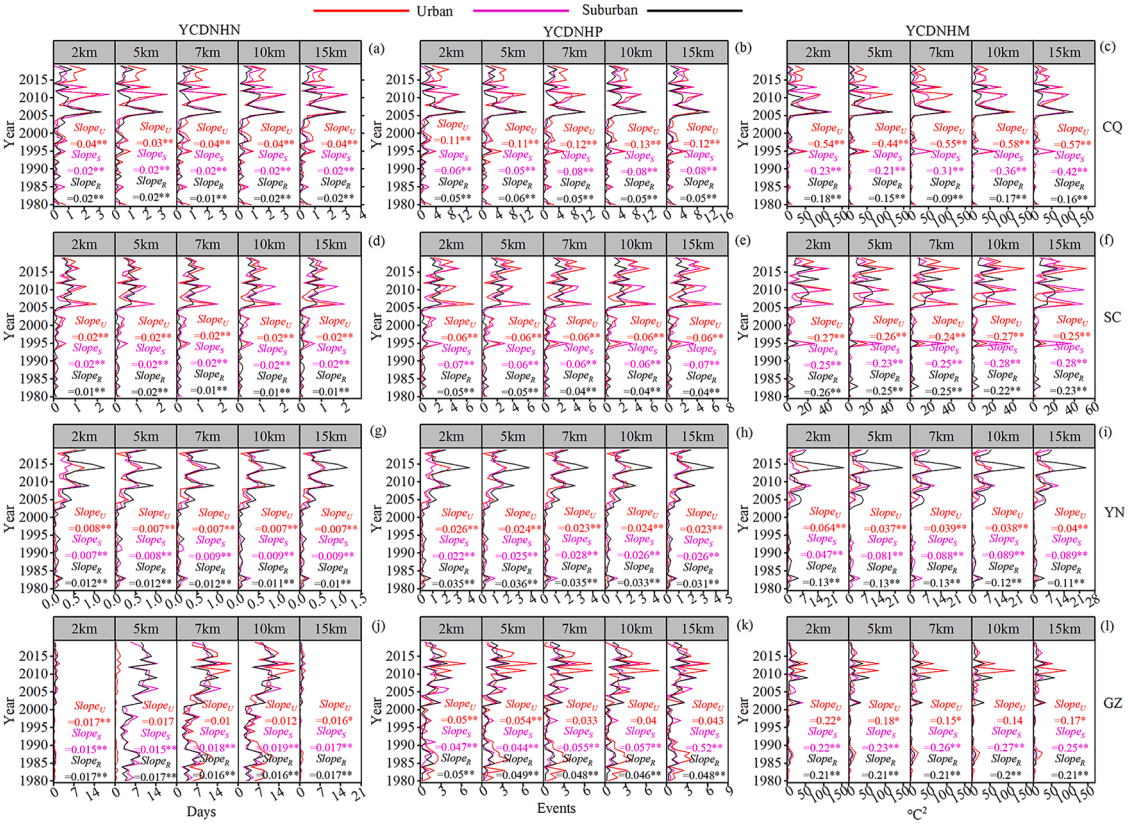


**Fig. 17.** Dynamic temporal characteristics of heatwaves indices (YCDNHN, YCDNHP, and YCDNHM) for different buffer areas based on surface temperature.

**Table 3**
Spatial evolution heatwaves (for YCDNHM index) persistent events using DBSCN based on air temperature.

| | Start date | End date | Duration | Average YCDNHM | Max YCDNHM | Max YCDNHM occurrence date |
|---|---|---|---|---|---|---|
| 1 | 1980–06–29 | 1980–07–03 | 4 | 1.42 | 2.21 | 1980–7–2 |
| 2 | 1985–10–10 | 1985–10–17 | 7 | 3.72 | 5.91 | 1985–10–13 |
| 3 | 1987–02–13 | 1987–02–16 | 3 | 4.29 | 8.20 | 1987–02–16 |
| 4 | 1988–05–02 | 1988–05–08 | 6 | 5.23 | 11.20 | 1988–05–06 |
| 5 | 2002–07–13 | 2002–07–18 | 5 | 1.99 | 2.96 | 2002–07–16 |
| 6 | 2002–10–16 | 2002–10–19 | 3 | 1.84 | 2.71 | 2002–10–19 |
| 7 | 2003–09–25 | 2003–09–28 | 3 | 0.96 | 1.51 | 2003–09–27 |
| 8 | 2005–11–03 | 2005–11–08 | 5 | 4.46 | 8.91 | 2005–11–05 |
| 9 | 2006–11–09 | 2006–11–13 | 4 | 2.05 | 2.99 | 2006–11–13 |
| 10 | 2009–03–18 | 2009–03–23 | 5 | 6.44 | 12.93 | 2009–03–21 |
| 11 | 2009–09–05 | 2009–09–15 | 10 | 3.05 | 6.33 | 2009–09–09 |
| 12 | 2011–09–16 | 2011–09–19 | 3 | 1.45 | 2.94 | 2011–09–17 |
| 13 | 2013–01–30 | 2013–02–07 | 8 | 10.35 | 17.18 | 2013–01–31 |
| 14 | 2014–01–30 | 2014–02–05 | 6 | 6.20 | 14.56 | 2014–01–31 |
| 15 | 2014–04–15 | 2014–04–19 | 4 | 3.22 | 6.07 | 2014–04–18 |
| 16 | 2015–01–23 | 2015–01–28 | 5 | 3.14 | 4.41 | 2015–01–24 |
| 17 | 2016–07–08 | 2016–07–12 | 4 | 1.22 | 2.46 | 2016–07–09 |
| 18 | 2016–08–17 | 2016–08–26 | 9 | 2.51 | 5.87 | 2016–08–25 |
| 19 | 2019–06–07 | 2019–06–13 | 6 | 1.84 | 3.06 | 2019–06–10 |
| 20 | 2019–08–18 | 2019–08–22 | 4 | 1.06 | 2.06 | 2019–08–20 |

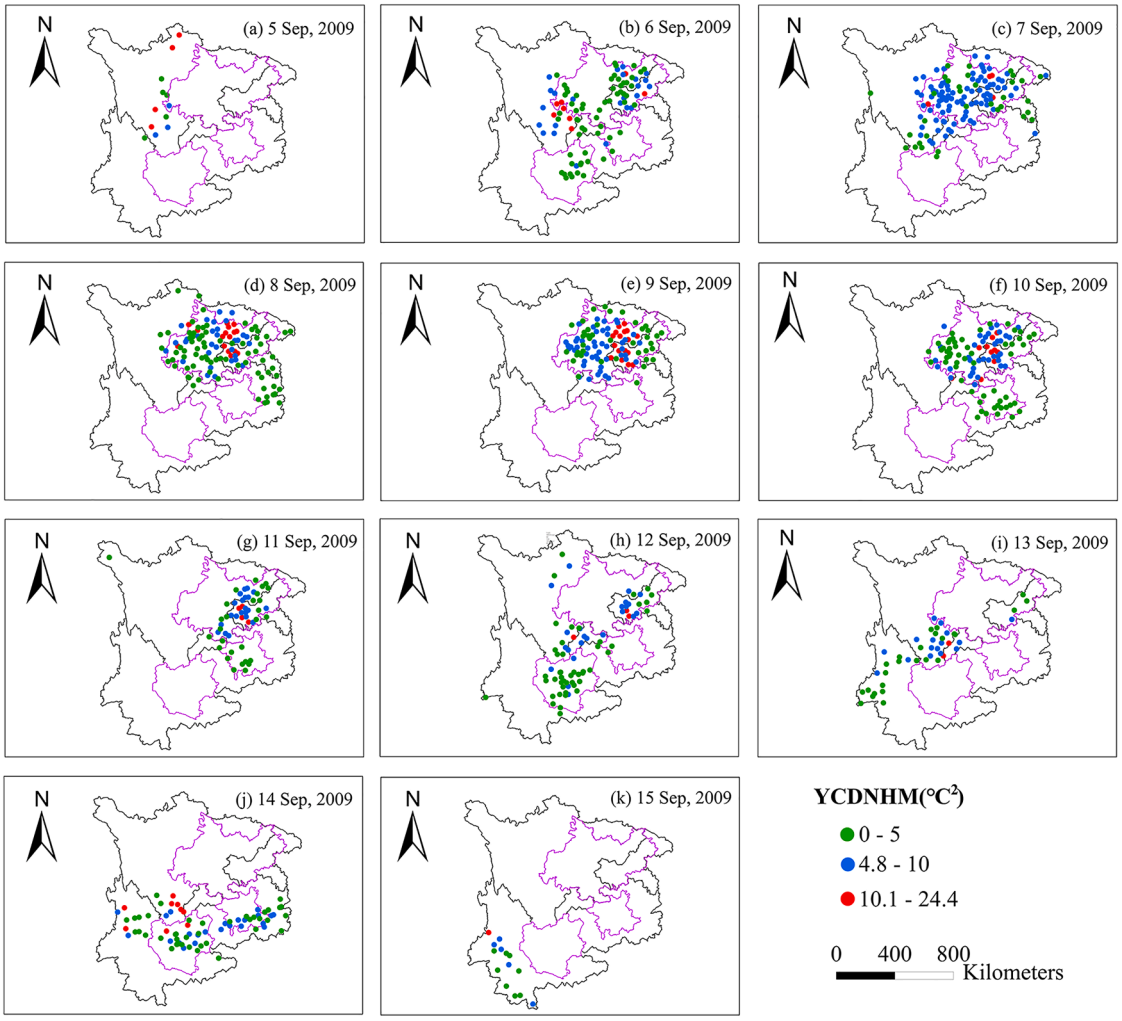


**Fig. 18.** Temporal and spatial evolution of heatwaves events of clustered hot stations for the most extreme regional heatwave event during 1980–2019 in SouthwestChina that persisted from 5 to 15 September 2009 based on air temperature data.

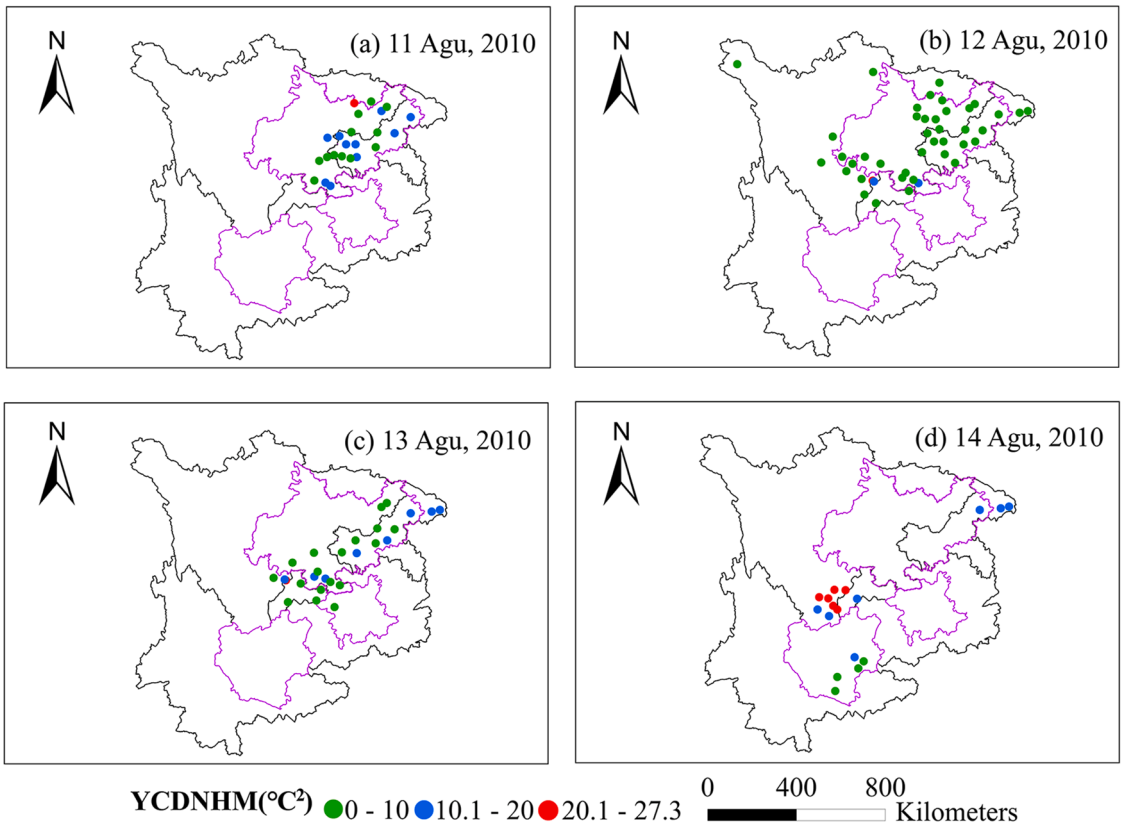


**Fig. 19.** Temporal and spatial evolution of heatwaves events of clustered hot stations for the most extreme regional heatwaves event during 1980–2019 in Southwest China that persisted from 11 to 14 August 2010 based on surface temperature data.

**Table 4**
Spatial evolution heatwave (YCDNHM) persistent events using DBSCN based on surface temperature.

| | Start date | End date | Duration | Average YCDNHM | Max YCDNHM | Max YCDNHM occurrence date |
|---|---|---|---|---|---|---|
| 1 | 2009–02–12 | 2009–02–15 | 3 | 11.45 | 14.55 | 2009–2–12 |
| 2 | 2010–08–11 | 2010–08–14 | 3 | 5.26 | 6.92 | 2010–08–14 |
| 3 | 2016–03–05 | 2016–03–08 | 3 | 9.47 | 14.57 | 2016–03–07 |

## 4. Discussion

### *4.1. Methods of uncertainty in classifying urban, suburban, and rural stations*

The accurate classification of station types revealed that heatwave differences among urban, suburban, and rural areas are critical for understanding different regions and taking targeted heatwaves measures. Previous studies have generally used absolute or relative threshold classification methods based on land use and land cover (nighttime light) data and only classified urban and rural heatwaves using air temperatures in a single specific buffer zone (Liao et al., 2018; Luo & Lau, 2019; Tysa et al., 2019; Yang et al., 2017; Ma et al., 2021; Shi et al., 2021; Wu et al., 2020). In this studies, our calculated intensities, durations, and magnitudes of heatwaves in urban, suburban, and rural areas obtained using different buffer zones were obviously different. According to the absolute threshold classification method, the number of urban, suburban, and rural stations changed greatly from 1980 to 2019, while when using the relative threshold classification method, the numbers of urban and suburban stations fluctuated less from 1980 to 2019, but the urban coverage ratio changed significantly among different time periods and buffer zones in Southwest China. Furthermore, the correlations of maximum and minimum air and surface temperature with urban expansion rate of each station with different buffer zones were different. The results showed that the urban expansion rate was significantly correlated with both average and minimum air temperature, and the correlation coefficient increased with increasing buffer zone radius, but had no significant correlation with the average maximum and minimum surface temperature. This showed that different station classification methods and different data types of quantitative heatwaves may have a significant impact on the results. Moreover, due to regional heterogeneity, we did not find strong correlations for some buffer sizes were used in previous studies (Yang et al., 2017;Tysa et al., 2019), which may be related to the complex terrain and different buffer areas. It can be seen that in the field of heatwaves research, various quantitative identification methods still need to be further developed to accurately quantify the difference of heatwaves changes in urban, suburban, and rural areas. At the same time, our methods also need to be validated in further similar research.

### *4.2. Spatiotemporal change of heatwaves*

Based on both air and surface temperature, the slopes of YDTN, YNTN, YCDNN, YCDNHN, YCDNHP, and YCDNM significantly increased over the study period. According to the heatwaves indices calculated using air temperature, 94.88%, 89.76%, and 93.98% of the stations exhibited significant increases in DYT, NGT, and CDNG indices, respectively, and when using surface temperature, 56.9%, 94.28%, and

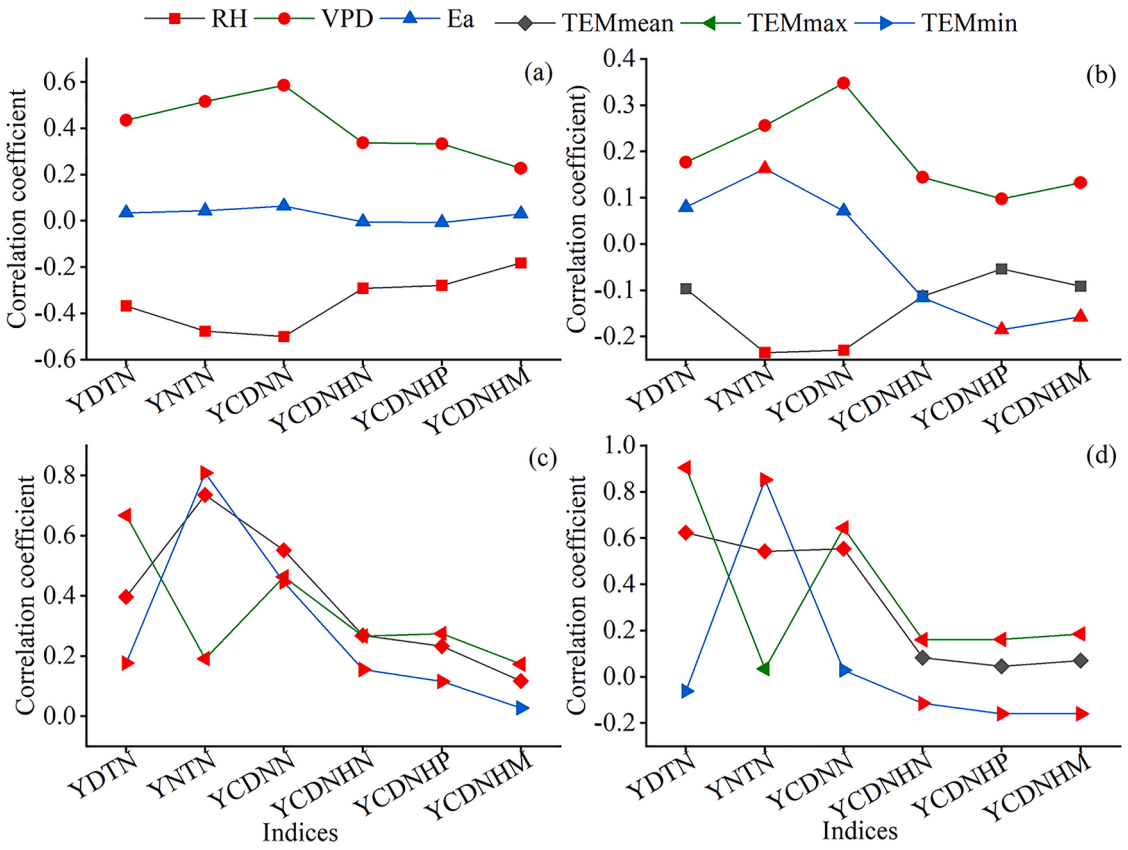


**Fig. 20.** Correlations between the slopes of heatwave indices of air (a) and surface (b) temperature and the slopes of relative humidity (RH), atmospheric water vapor pressure (Ea), vapor pressure deficit (VPD), (c) average, maximum, and minimum air temperature, and (d) average, maximum, and minimum surface temperature (red dots denote significance at $p < 0.05$).

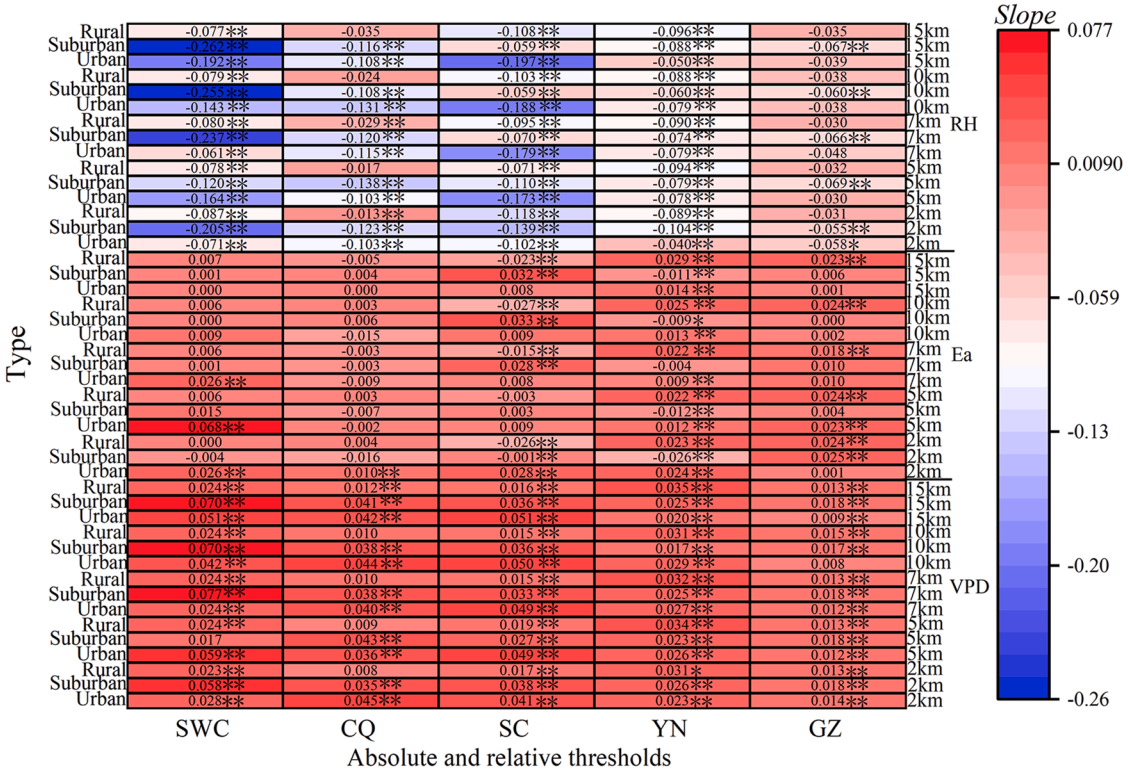


**Fig. 21.** Heatmap of relative humidity (RH), atmospheric water vapor pressure (Ea), and vapor pressure deficit (VPD) change trends during 1980–2019.

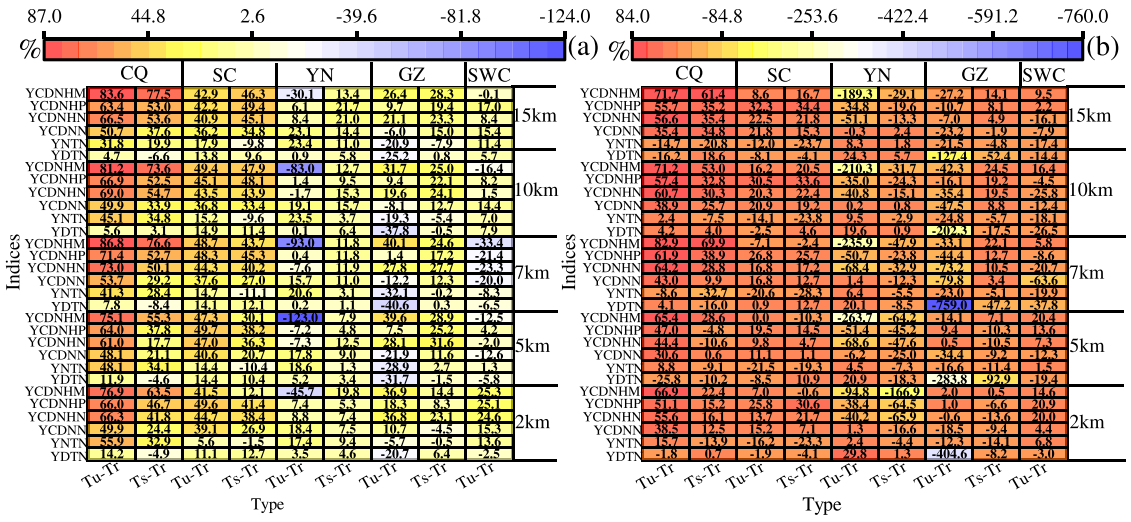


**Fig. 22.** Urbanization effects on (a) air and (b) surface temperatures based on heatwaves in Southwest China during 1980–2019 based on relative (CQ, SC, YN, and GZ) and absolute (SWC) threshold classifications using different buffer area sizes.

82.15% increased significantly, showing the obvious increasing trends in heatwaves across Southwest China. These findings were similar to the observations by Deng et al. (2020) in Southwest China, Huang et al. (2021) in Sichuan Basin, and Wu et al. (2020) and Yu et al. (2021) in China in summer for air temperature. However, the findings were inconsistent with An and Zuo (2021) who found the change in DYT heatwaves was insignificant in China, which may have been because our study considered the whole year in calculating the heatwaves indices while An and Zuo (2021) focused on summer (June to August) for air temperature. Meanwhile, it should also be noted here that the six calculated heatwaves indices were significantly different overall due to the significantly different numbers of urban, suburban, and rural stations when using different sizes of buffer zones and different classification methods, the differences in suburban stations were especially large and there were significantly more suburban stations when classified by relative thresholds than by absolute thresholds. Furthermore, the topography of Southwest China is complex, and although we used all suitable stations (more than 400 stations), we still excluded more than 80 stations for air temperature and 100 stations for surface temperature that did not meet the quality requirements. Therefore, our calculated trends in heatwaves indices for urban, suburban, and rural stations should be regarded as conservative estimates. In addition, differences among the study areas may also lead to different results. The comprehensive air and surface temperature heatwaves indices showed that the increasing trends in NGT heatwaves were obvious and probably dominated the increases in CDNG heatwaves. These results were consistent with China (An & Zuo, 2021; Chen et al., 2017) and the Northern Hemisphere (Wang et al., 2020) for summer. This means that compound heat extremes have become the most common type of heatwaves across the northern continents (Vogel et al., 2019; Wang et al., 2020). Furthermore, our study, considering all days of the year (365 or 366t days) and using the 90% threshold, extracted DYT, NGT, and CDNG heatwaves events for urban, suburban, and rural areas using different buffer areas based on absolute and relative thresholds. The results showed that, whether based on absolute or relative thresholds, urban, suburban, and rural heatwaves exhibited significant increasing trends, and the amplitudes of the increases at urban and suburban stations were greater than at rural stations using either air and surface temperature based on absolute threshold, which was also consistent with previous research (Liao et al., 2018; Ma & Yuan, 2021; Shi et al., 2021). Meanwhile, according to relative threshold methods, we found that not all heatwaves indices produced the urban>suburban>rural order for all buffer area sizes, for example, the orders were rural>suburban>urban and suburban>rural>urban for some heatwaves indices in YN and GZ, which agreed with Luo and Lau (2021) and Wang et al. (2021a) who found that the impacts of urbanization were negative and cooling in the central GZ and YN urban agglomerations based on a 33% absolute threshold for heat stress. This clearly showed that the methods for classifying different station types and the buffer area sizes strongly affect the results based on relative and absolute thresholds. At present, there is no consensus on which buffer area is most appropriate for identifying stations as urban, suburban, or rural, which is especially important for suburban areas. Our results also showed that the relative threshold classification method based on different socioeconomic development levels (i.e., built-up areas) of each region was obviously different when using absolute threshold. Logically, considering regional climates and socioeconomic development levels, it may be more reasonable to use the relative threshold station classification method. However, its application in other regions still needs to be verified through comparisons of the relative and absolute threshold methods.

Further, based on the DBSCN method, we extracted the top three ranking spatially persistent heatwaves events, which occurred in September 2009, February 2013, and August 2016. As we know, from 2009 to 2012, the four provinces (i.e., YN, SC, CQ, GZ, and Guangxi provinces) and municipality (i.e., Chongqing) in Southwest China suffered extreme “Autumn–Winter–Spring” droughts (Sun et al., 2016) and, generally speaking, high temperatures occurred together with drought. Meanwhile, high summer temperatures in SC and CQ in 2016 (http://www.weather.com.cn/) and a warm winter event was also reported in YN at 2012/2013, the highest since 1961 (https://www.yunnan.cn/). In addition, we also observed continuous heatwaves events in 2019, during which the mean rainfall deficit during March–June 2019 was the worst since 1961 and the hottest temperature on record for YN occurred (Wang et al., 2021b). In short, the heatwaves events in Southwest China increased in magnitude, frequency, intensity, and duration in both urban and rural stations along with the rest of China (Chen et al., 2021; An & Zuo, 2021; Liao et al., 2018;; Shi et al., 2021; Wu et al., 2020), especially in SC and CQ.

### 4.3. *Impact factor*

Southwest China has suffered from an increasing frequency of summer heatwaves in recent years (Deng et al., 2020). However, due to the differences of regional socioeconomic development and physical geography, the changes and impacts of heatwaves in different regions are different. However, it is clear that the relative humidity, vapor pressure

deficit, and evapotranspiration between urban and rural areas were obviously different (Shi et al., 2021). We found heatwaves indices based on air and surface temperature were significantly positively/negative correlated with vapor pressure deficit/relative humidity, which may indicate that the differences in heatwaves between urban, suburban, and rural areas result from differences in these meteorological factors. Meanwhile, we found urbanization had a negative effect on heatwaves based on relative (YN, GZ) and absolute (SWC) thresholds for different buffer zones. This phenomenon was also observed by Luo and Lau (2021) and Wang et al. (2021a) in Central YN and Central GZ using 2 km buffer areas, whilst Luo and Lau (2021) saw that local urbanization in Central YN increased the decline in relative humidity by 0.26%/decade, accounting for 49.3% of the decreasing humidity trend in Central YN urban regions. In this situation, the reduced heat stress resulting from lower humidity likely outweighed the intensifying effect from higher temperatures, resulting in lower overall midsummer heat stress in Central YN. At the same time, for the differences in heatwaves between DYT and NGT, as observed by Arshad et al. (2021), solar radiation is absorbed by buildings, impermeable surfaces, and bare soils throughout the day and thermal emissions are released heat at night, causing air temperature in urban areas to remain high at night while air temperature in rural locations decreases. In an urban agglomeration, Luo and Lau (2021) observed a strong urban dry island effect characterized by lower humidity and a higher vapor pressure deficit in the urban core. Rapid urban land growth has considerably exacerbated the dry island effect in recent decades. Around half of the decrease in atmospheric humidity and increase in vapor pressure deficit in urban regions could be attributed to urban expansion. Meanwhile, Shi et al. (2021) revealed that urbanization was responsible for almost half of the increase in duration and nearly 40% of the increases in severity and frequency of NGT heatwaves in urban regions compared to rural. The nocturnal urban heat island results from urban growth, which lowers evapotranspiration and diminishes wind speed, which would typically cool the lower atmosphere through turbulent heat loss and cooled air advection (Shi et al., 2021). In addition, various large-scale circulation processes also had important effects on heatwaves in Southwest China, including the Arctic sea ice, North Pacific subtropical high (Deng et al., 2020; Yu et al., 2021), the mid-to-upper-level height anomalies over western Europe, tropical convection anomalies, enhanced Philippine Sea convection, and suppressed tropical eastern Indian Ocean convection (Huang et al., 2021).

Furthermore, differences in regional topography and geomorphology (such as the dry and hot valley in YN and basin in SC) cannot be ignored. These aforementioned factors may result in differences in the how heatwaves change in urban, suburban, and rural areas in Southwest China.

### 4.4. Limitations and uncertainties

There are some limitations to our study, although we excluded data prior to 1980 in order to retain as many stations as possible, more than 80 (100) stations were omitted due to strict quality requirements for air (surface) temperature, which may have affected the numbers of stations classified as urban, suburban, and rural. Also, we did not classify the buffer zones at 1 km intervals, and when using Spearman correlations between the proportion of built-up area expansion with the slopes of the mean, maximum, and minimum air and surface temperature, we did not find that any correlation was best for a particular buffer zone, but rather the correlation coefficient increased as the buffer zone increased. Further, despite our effort to ensure quality data in the station classification approach, the station classification requirements may need to be further improved. For example, Li et al. (2019b) developed relatively strict urban/rural classification standards that eliminated the influences of various factors (i.e., inland lakes, ponds, rivers, water bodies, highways or railways, etc.). Further, the spatial persistence approach should also consider comparing dynamically changing indicator semi-variograms (Zhou et al., 2021b). Tysa et al. (2019) also pointed out that land use statistics for current observational stations are still being collected, resulting in mismatches between urban warming rates and percentages of urban land use around the observation stations. Urban indicators should be expanded to include the precise locations of previous observational stations as well as the nonlinear aspects of urban land use variability.

In summary, the urbanization impacts of heatwaves events, using air and surface temperatures, assessed using absolute and relative thresholds were obviously different when using different buffer zone sizes, especially in suburban areas. Therefore, further exploration is needed in terms of data time resolution (hourly heatwave analysis), station type classification method, buffer zone size, spatial heatwaves events identification, and so forth to provide more powerful scientific reference values for urban planners and decision makers. These limitations, relevant to both data and methodology, need to be further considered in future studies.

## 5. Conclusions

Using dynamic classifications of urban, suburban, and rural stations based on high-resolution (30 m) land use and cover data, this study investigated the changes in long-term trends of daytime, nighttime, and concurrent daytime and nighttime heatwave characteristics based on daily air and surface temperature $T_{max}$ and $T_{min}$ data sets for six heatwaves indices during 1980–2019 from over 300 (197) meteorological stations in Southwest China. The main conclusions are as follows:

(1) The classification methods for urban, suburban, and rural stations performed differently, which had an obvious influence on the transfer of rural stations to urban (suburban) and suburban stations to urban stations. According to the absolute threshold, many stations changed from rural to suburban and from rural or suburban to urban. However, according to the relative threshold, relatively few stations changed from rural to suburban or from suburban to urban.

(2) The spatiotemporal changes of heatwave indices performance based on air and surface temperature were obviously different, therefore, the results based on different data sources should be used carefully when evaluating heat wave changes. Specifically, all six heatwave indices based on air and surface temperature showed significant upward and abrupt changes during 1980–2019. Furthermore, the magnitudes of the trends using surface temperature were larger than when using air temperature for the six heatwaves indices, except surface temperature $<$ air temperature for YNTN. The general spatial patterns for air and surface temperature heatwaves were same, whereas the number of stations with increasing trend magnitudes were more when using air and surface temperature for YCDNHN, YCDNHP, and YCDNHM. Furthermore, the regional heatwaves events occurred more frequently when identified using air temperature than when identified by surface temperature. Finally, in the years when heatwaves events were jointly identified using both data sets, the dates of the events were also significantly different.

(3) Classification urban (suburban) and rural stations based on absolute and relative thresholds reveals that the impact of urbanization in different buffer zones is obviously different. Therefore, another important consideration for methodology is determining which size of buffer zone is more suitable for classifying urban (suburban) and rural stations, for which further exploration is needed. In our study, we found that the impacts of urbanization (warming or cooling) quantified based on air and surface temperature were obviously different when using different buffer zone sizes, especially in suburban areas (for air temperature, suburban areas had a greater cooling impact than for surface

temperature). Overall, urbanization has accelerated heatwaves intensification, especially CDNG heatwaves events.

## CRediT authorship contribution statement

**Qingping Cheng:** Conceptualization, Methodology, Validation, Writing – original draft, Funding acquisition, Writing – review & editing. **Hanyu Jin:** Methodology, Validation. **Yitong Ren:** Formal analysis, Data curation, Writing – review & editing.

## Declaration of Competing Interest

The authors declare no conflicts of interest.

## Data availability

The data that has been used is confidential.

## Acknowledgment

This study was supported by the Yunnan Fundamental Research Projects (Grant no. 202201AU070064), Southwest Forestry University Research Initiation Project (112105), and Strategic Priority Research Program of the Chinese Academy of Sciences (Grant no. XDA20100104).

## Supplementary materials

Supplementary material associated with this article can be found, in the online version, at doi:10.1016/j.scs.2023.104433.

## References

An, N., & Zuo, Z. (2021). Changing structures of summertime heatwaves over China during 1961–2017. *Science China Earth Sciences, 64*, 1242–1253. https://doi.org/10.1007/s11430-020-9776-3

Arnfield, A. J. (2003). Two decades of urban climate research: A review of turbulence, exchanges of energy and water, and the urban heat island. *International Journal of Climatology, 23*, 1–26. https://doi.org/10.1002/joc.859

Arshad, M., Khedher, K. M., Eid, E. M., & Aina, Y. A. (2021). Evaluation of the urban heat island over Abha-Khamis Mushait tourist resort due to rapid urbanisation in Asir, Saudi Arabia. *Urban Climate, 36*, Article 100772. https://doi.org/10.1016/j.uclim.2021.100772

Cai, W., Zhang, C., Suen, H.P., .Ai, S., Bai, Y., Bao, J., Di, Q. (2020). The 2020 China report of the lancet countdown on health and climate change.

Chen, K., Bi, J., Chen, J., Chen, X., Huang, L., & Zhou, L. (2015). Influence of heat wave definitions to the added effect of heatwaves on daily mortality in Nanjing, *China. Science of the Total Environment, 506-507*, 18–25. https://doi.org/10.1016/j.scitotenv.2014.10.092

Chen, X., Li, N., Liu, J., Zhang, Z., Liu, Y., & Huang, C. (2020). Changes in global and regional characteristics of heat stress waves in the 21st century. *Earth's Future, 8*(11), 1–17. https://doi.org/10.1029/2020EF001636

Chen, Y., & Zhai, P. (2017). Revisiting summertime hot extremes in China during 1961–2015: Overlooked compound extremes and significant changes. *Geophysical Research Letters, 44*(10), 5096–5103. https://doi.org/10.1002/2016GL072281

Chongqing Meteorological Bureau. (2021). Weather service column. http://cq.cma.gov.cn/sqxj/qxfw.

Christidis, N., Jones, G. S., & Stott, P. A. (2015). Dramatically increasing chance of extremely hot summers since the 2003 European heatwave. *Nature Climate Change, 5*(1), 46–50. https://doi.org/10.1038/nclimate2468

Chuan, T., Wu, J., Zhao, D., Yang, Q., Fan, W., & Zhao, J. (2022). Fine structure analysis of urban heat island of a central city in low-latitude plateau of China. *Urban Climate, 44*, Article 101186. https://doi.org/10.1016/j.uclim.2022.101186

Deng, K., Jiang, X., Hu, C., & Chen, D. (2020). More frequent summer heatwaves in southwestern China linked to the recent declining of Arctic sea ice. *Environmental Research Letters, 15*(7), Article 074011. https://doi.org/10.1088/1748-9326/ab8335

Ester, M., Kriegel, H.-. P., Sander, J., & Xu, X. (1996). A density-based algorithm for discovering clusters in large spatial databases with noise. In *Proceedings of the 2nd International Conference on Knowledge Discovery and Data Mining*.

Frölicher, T. L., Fischer, E. M., & Gruber, N. (2018). Marine heatwaves under global warming. *Nature, 560*(7718), 360–364. https://doi.org/10.1038/s41586-018-0383-9

He, B. J., Ding, L., & Prasad, D. (2020). Wind-sensitive urban planning and design: Precinct ventilation performance and its potential for local warming mitigation in an open midrise gridiron precinct. *Journal of Building Engineering, 29*, Article 101145. https://doi.org/10.1016/j.jobe.2019.101145. Article.

He, B. J., Zhao, D., Xiong, K., Qi, J., Ulpiani, G., Pignatta, G., et al. (2021). A framework for addressing urban heat challenges and associated adaptive behaviour by the public and the issue of willingness to pay for heat resilient infrastructure in Chongqing, China. *Sustainable Cities and Society, 103361*. https://doi.org/10.1016/j.scs.2021.103361. Article.

Huang, W., Kan, H., & Kovats, S. (2010). The impact of the 2003 heat wave on mortality in Shanghai, China. *Science of the Total Environment, 408*(11), 2418–2420. https://doi.org/10.1016/j.scitotenv.2010.02.009

Huang, X., Zhang, T., Jiang, X., Liu, S., & Xiao, D. (2021). Interannual variability of mid-summer heat wave frequency over the Sichuan Basin. *International Journal of Climatology, 41*(10), 5036–5050. https://doi.org/10.1002/joc.7115

Jamei, Y., Rajagopalan, P., & Sun, Q. (2019). Spatial structure of surface urban heat island and its relationship with vegetation and built-up areas in Melbourne, *Australia. Science of the Total Environment, 659*, 1335–1351. https://doi.org/10.1016/j.scitotenv.2018.12.308

Jiang, S., Lee, X., Wang, J., & Wang, K. (2019). Amplified urban heat islands during heat wave periods. *Journal of Geophysical Research: Atmospheres, 124*(14), 7797–7812. https://doi.org/10.1029/2018JD030230

Kim, H., Kim, H., Byun, G., Choi, Y., Song, H., & Lee, J. T. (2019). Difference in temporal variation of temperature-related mortality risk in seven major South Korean cities spanning 1998–2013. *Science of the Total Environment, 656*, 986–996. https://doi.org/10.1016/j.scitotenv.2018.11.210

Kong, D., Gu, X., Li, J., Ren, G., & Liu, J. (2020). Contributions of global warming and urbanization to the intensification of human-perceived heatwaves over *China. Journal of Geophysical Research: Atmospheres, 125*(18). https://doi.org/10.1029/2019JD032175. e2019JD032175.

Larcom, S., She, P. W., & van Gevelt, T. (2019). The UK summer heatwave of 2018 and public concern over energy security. *Nature Climate Change, 9*(5), 370–373. https://doi.org/10.1038/s41558-019-0460-6

Li, D., Sun, T., Liu, M., Wang, L., & Gao, Z. (2016). Changes in wind speed under heatwaves enhance urban heat islands in the Beijing metropolitan area. *Journal of Applied Meteorology and Climatology, 55*(11), 2369–2375. https://doi.org/10.1175/JAMC-D-16-0102.1

Li, X., Li, Y., Chen, A., Gao, M., Slette, I. J., & Piao, S. (2019a). The impact of the 2009/2010 drought on vegetation growth and terrestrial carbon balance in Southwest China. *Agricultural and Forest Meteorology, 269*, 239–248. https://doi.org/10.1016/j.agrformet.2019.01.036

Li, X., Ren, G., Wang, S., You, Q., Sun, Y., Ma, Y., & Zhang, W. (2021). Change in the heatwave statistical characteristics over China during the climate warming slowdown. *Atmospheric Research, 247*, Article 105152. https://doi.org/10.1016/j.atmosres.2020.105152

Li, Y., Wang, L., Zhou, H., Zhao, G., Ling, F., Li, X., et al. (2019b). Urbanization effects on changes in the observed air temperatures during 1977–2014 in China. *International Journal of Climatology, 39*(1), 251–265. https://doi.org/10.1002/joc.5802

Liao, S., Cai, H., Tian, P., Zhang, B., & Li, Y. (2022). Combined impacts of the abnormal and urban heat island effect in Guiyang, a typical Karst Mountain City in China. *Urban Climate, 41*, Article 101014. https://doi.org/10.1016/j.uclim.2021.101014

Liao, W., Liu, X., Li, D., Luo, M., Wang, D., Wang, S., & Yang, X. (2018). Stronger contributions of urbanization to heat wave trends in wet climates. *Geophysical Research Letters, 45*(20), 11310–11317. https://doi.org/10.1029/2018GL079679

Liu, X., Tian, G., Feng, J., Hou, H., & Ma, B. (2022). Adaptation strategies for urban warming: Assessing the impacts of heat waves on cooling capabilities in Chongqing, China. *Urban Climate, 45*, Article 101269. https://doi.org/10.1016/j.uclim.2022.101269

Lu, R., Xu, K., Chen, R., Chen, W., Li, F., & Lv, C. (2022). Heat waves in summer 2022 and increasing concern regarding heat waves in general. *Atmospheric and Oceanic Science Letters.* , Article 100290. https://doi.org/10.1016/j.aosl.2022.100290

Luo, M., & Lau, N. C. (2019). Urban expansion and drying climate in an urban agglomeration of East China. *Geophysical Research Letters, 46*(12), 6868–6877. https://doi.org/10.1029/2019GL082736

Luo, M., & Lau, N. C. (2021). Increasing human-perceived heat stress risks exacerbated by urbanization in China: A comparative study based on multiple metrics. *Earth's Future, 9*(7). https://doi.org/10.1029/2020EF001848. e2020EF001848.

Ma, F., & Yuan, X. (2021). More persistent summer compound hot extremes caused by global urbanization. *Geophysical Research Letters, 48*(15). https://doi.org/10.1029/2021GL093721. e2021GL093721.

Mann, H. B. (1945). Nonparametric tests against trend. *Econometrica: Journal of the Econometric Society, 133*, 245–259. https://doi.org/10.2307/1907187

Manoli, G., Fatichi, S., Schläpfer, M., Yu, K., Crowther, T. W., Meili, N., & Bou-Zeid, E. (2019). Magnitude of urban heat islands largely explained by climate and population. *Nature, 573*, 55–60. https://doi.org/10.1038/s41586-019-1512-9

Marzban, F., Sodoudi, S., & Preusker, R. (2018). The influence of land-cover type on the relationship between NDVI–LST and LST-Tair. *International Journal of Remote Sensing, 39*(5), 1377–1398. https://doi.org/10.1080/01431161.2017.1402386

Murage, P., Hajat, S., & Kovats, R. S. (2017). Effect of night-time temperatures on cause and age-specific mortality in London. *Environmental Epidemiology, 1*(2), e005. https://doi.org/10.1097/EE9.0000000000000005

National Bureau of Statistics of the People's Republic of China. (2021). *China statistical yearbook* (pp. 1–945). China Statistics Press.

Panda, D. K., AghaKouchak, A., & Ambast, S. K. (2017). Increasing heatwaves and warm spells in India, observed from a multiaspect framework. *Journal of Geophysical Research: Atmospheres, 122*(7), 3837–3858. https://doi.org/10.1002/2016JD026292

Pettitt, A. N. (1979). A non-parametric approach to the change-point problem. *Journal of the Royal Statistical Society: Series C (Applied Statistics), 28*(2), 126–135. https://doi.org/10.2307/2346729

Qin, N., Chen, X., Fu, G., Zhai, J., & Xue, X. (2010). Precipitation and temperature trends for the Southwest China: 1960–2007. *Hydrological processes, 24*(25), 3733–3744. https://doi.org/10.1002/hyp.7792

Rastogi, D., Lehner, F., & Ashfaq, M. (2020). Revisiting recent US heatwaves in a warmer and more humid climate. *Geophysical Research Letters, 47*(9). https://doi.org/10.1029/2019gl086736. e2019GL086736.

Ren, G., Li, J., Ren, Y., Chu, Z., Zhang, A., Zhou, Y., & Bian, T. (2015). An integrated procedure to determine a reference station network for evaluating and adjusting urban bias in surface air temperature data. *Journal of Applied Meteorology and Climatology, 54*(6), 1248–1266. https://doi.org/10.1175/JAMC-D-14-0295.1

Ren, G. Y. (2012). Climate change and the engineering projects of the Qinghai-Tibet Plateau. *Engineering Sciences, 14*, 89–95.

Russo, S., Dosio, A., Graversen, R. G., Sillmann, J., Carrao, H., Dunbar, M. B., & V. ogt, J. V. (2014). Magnitude of extreme heatwaves in present climate and their projection in a warming world. *Journal of Geophysical Research: Atmospheres, 119*(22), 12–500. https://doi.org/10.1002/2014jd022098

Ruuhela, R., Hyvärinen, O., & Jylhä, K. (2018). Regional assessment of temperature-related mortality in Finland. *International journal of environmental research and public health, 15*(3), 406. https://doi.org/10.3390/ijerph15030406

Sen, P. K. (1968). Estimates of the regression coefficient based on Kendall's tau. *Journal of the American Statistical Association, 63*(324), 1379–1389. https://doi.org/10.1080/01621459.1968.10480934

Shi, Z., Xu, X., & Jia, G. (2021). Urbanization magnified nighttime heatwaves in China. *Geophysical Research Letters, 48*(15). https://doi.org/10.1029/2021GL093603. e2021GL093603.

Su, Q., & Dong, B. (2019a). Recent decadal changes in heatwaves over China: Drivers and mechanisms. *Journal of Climate, 32*(14), 4215–4234. https://doi.org/10.1175/JCLI-D-18-0479.1

Su, Q., & Dong, B. (2019b). Projected near-term changes in three types of heatwaves over China under RCP4. 5. *Climate Dynamics, 53*(7), 3751–3769. https://doi.org/10.1007/s00382-019-04743-y

Sun, X., Sun, Q., Yang, M., Zhou, X., Li, X., Yu, A., & Guo, Y. (2014a). Effects of temperature and heatwaves on emergency department visits and emergency ambulance dispatches in Pudong New Area, China: A time series analysis. *Environmental Health, 13*(1), 1–8. https://doi.org/10.1186/1476-069x-13-76

Sun, Y., Song, L., Yin, H., Zhang, X., Stott, P., Zhou, B., et al. (2016). Human influence on the 2015 extreme high temperature events in Western China. *Bulletin of the American Meteorological Society, 97*(12), S102–S106. https://doi.org/10.1175/BAMS-D-16-0158.1

Sun, Y., Zhang, X., Zwiers, F. W., Song, L., Wan, H., Hu, T., & Ren, G. (2014b). Rapid increase in the risk of extreme summer heat in Eastern China. *Nature Climate Change, 4*(12), 1082–1085. https://doi.org/10.1038/nclimate2410

Theil, H. (1950). A rank-invariant method of linear and polynomial regression analysis. *Indagationes Mathematicae, 12*, 173. https://doi.org/10.1007/978-94-011-2546-8_20

Todd, N., & Valleron, A. J. (2015). Space–time covariation of mortality with temperature: A systematic study of deaths in France, 1968–2009. *Environmental Health Perspectives, 123*(7), 659–664. https://doi.org/10.1289/ehp.1307771

Tysa, S. K., Ren, G., Qin, Y., Zhang, P., Ren, Y., Jia, W., et al. (2019). Urbanization effect in regional temperature series based on a remote sensing classification scheme of stations. *Journal of Geophysical Research: Atmospheres, 124*(20), 10646–10661. https://doi.org/10.1029/2019JD030948

Varentsov, M. I., Grishchenko, M. Y., & Wouters, H. (2019). Simultaneous assessment of the summer urban heat island in Moscow megacity based on *in situ* observations, thermal satellite images and mesoscale modeling. *Geography, Environment, Sustainability, 12*(4), 74–95. https://doi.org/10.24057/2071-9388-2019-10

Vogel, M. M., Zscheischler, J., Wartenburger, R., Dee, D., & Seneviratne, S. I. (2019). Concurrent 2018 hot extremes across northern hemisphere due to human-induced climate change. *Earth's future, 7*(7), 692–703. https://doi.org/10.1029/2019EF001189

Wang, J., Chen, Y., Tett, S. F., Yan, Z., Zhai, P., Feng, J., et al. (2020). Anthropogenically-driven increases in the risks of summertime compound hot extremes. *Nature Communications, 11*(1), 1–11. https://doi.org/10.1038/s41467-019-14233-8

Wang, J., & Yan, Z. (2021). Rapid rises in the magnitude and risk of extreme regional heat wave events in China. *Weather and Climate Extremes, 34*, Article 100379. https://doi.org/10.1016/j.wace.2021.100379

Wang, L., Chen, ., Zhou, ., & Huang, G. (2015). Drought in Southwest China: A review. *Atmospheric and Oceanic Science Letters, 8*(6), 339–344. https://doi.org/10.31497/zrzyxb.20210508

Wang, P., Luo, M., Liao, W., Xu, Y., Wu, S., Tong, X., & Han, Y. (2021a). Urbanization contribution to human perceived temperature changes in major urban agglomerations of China. *Urban Climate, 38*(4), Article 100910. https://doi.org/10.1016/j.uclim.2021.100910

Wang, S., Huang, J., & Yuan, X. (2021b). Attribution of 2019 extreme spring–early summer hot drought over Yunnan in southwestern China. *Explaining Extreme Events of 2019 from a Climate Perspective Bulletin of the American Meteorological Society, 102*(1), S91–S96. https://doi.org/10.1175/BAMS-D-20-0121.1.

Wang, Y. W., Zhai, P. M., & Tian, H. (2006). Extreme high temperatures in southern China in 2003 under the background of climate change. *Meteorological Monthly, 32*(10), 27–33. https://doi.org/10.1016/S1003-6326(06)60040-X

Wu, X., Wang, L., Yao, R., Luo, M., Wang, S., & Wang, L. (2020). Quantitatively evaluating the effect of urbanization on heatwaves in China. *Science of the Total Environment, 731*, Article 138857. https://doi.org/10.1016/j.scitotenv.2020.138857

Xia, J., Chen, J., & Yu, D. X. (2022). Impacts and countermeasures of extreme drought in the Yangtze River Basin in 2022. *Journal of Hydraulic Engineering, 53*(10), 1143–1153. https://doi.org/10.13243/j.cnki.slxb.20220730 (in Chinese).

Xia, J., Tu, K., Yan, Z., & Qi, Y. (2016). The super-heat wave in eastern China during July–August 2013: A perspective of climate change. *International Journal of Climatology, 36*(3), 1291–1298. https://doi.org/10.1002/joc.4424

Xia, Y., Li, Y., Guan, D., Tinoco, D. M., Xia, J., Yan, Z., & Huo, H. (2018). Assessment of the economic impacts of heatwaves: A case study of Nanjing, *China. Journal of Cleaner Production, 171*, 811–819. https://doi.org/10.1016/j.jclepro.2017.10.069

Xiang, Y., Huang, C., Huang, X., Zhou, Z., & Wang, X. (2021). Seasonal variations of the dominant factors for spatial heterogeneity and time inconsistency of land surface temperature in an urban agglomeration of central China. *Sustainable Cities and Society, 75*, 103285. https://doi.org/10.1016/j.scs.2021.103285

Yang, X., Ruby Leung, L., Zhao, N., Zhao, C., Qian, Y., Hu, K., & Chen, B. (2017). Contribution of urbanization to the increase of extreme heat events in an urban agglomeration in east China. *Geophysical Research Letters, 44*(13), 6940–6950. https://doi.org/10.1002/2017GL074084

Yin, C., Yuan, M., Lu, Y., Huang, Y., & Liu, Y. (2018). Effects of urban form on the urban heat island effect based on spatial regression model. *Science of the Total Environment, 634*, 696–704. https://doi.org/10.1016/j.scitotenv.2018.03.350

Yin, Q., Wang, J., Ren, Z., Li, J., & Guo, Y. (2019). Mapping the increased minimum mortality temperatures in the context of global climate change. *Nature Communications, 10*(1), 1–8. https://doi.org/10.1038/s41467-019-12663-y

Yu, Y., Shao, Q., Lin, Z., & Kang, I. S. (2021). Characteristics Analysis and Synoptic Features of Event-Based Regional Heatwaves Over China. *Journal of Geophysical Research: Atmospheres, 126*(2). https://doi.org/10.1029/2020JD033865. e2020JD033865.

Zhang, X., Hegerl, G., Zwiers, F. W., & Kenyon, J. (2005). Avoiding inhomogeneity in percentile-based indices of temperature extremes. *Journal of Climate, 18*(11), 1641–1651. https://doi.org/10.1175/JCLI3366.1

Zhang, Y., Mao, G., Chen, C., Lu, Z., Luo, Z., & Zhou, W. (2020). Population exposure to concurrent daytime and nighttime heatwaves in Huai River Basin, China. *Sustainable Cities and Society, 61*, Article 102309. https://doi.org/10.1016/j.scs.2020.102309

Zhao, L. (2018). Urban growth and climate adaptation. *Nature Climate Change, 8*(12), 1034. https://doi.org/10.1038/s41558-018-0348-x

Zhou, H., Huang, X., Zhou, W., Zhang, Y., & Liu, Y. (2021b). Spatial correlation length of summer extreme heat stress over eastern China. *International Journal of Climatology, 41*(5), 3121–3138. https://doi.org/10.1002/joc.7009

Zhou, W., Huang, G., & Cadenasso, M. L. (2011). Does spatial configuration matter? Understanding the effects of land cover pattern on land surface temperature in urban landscapes. *Landscape and Urban Planning, 102*(1), 54–63. https://doi.org/10.1016/j.landurbplan.2011.03.009

Zhou,J. , Zhao, J.H. , Li,Y.H. , Zou, X.K. (2021a). Objective Identification and Variation Characteristics of Regional Heavy Rain-fall Events in the East of Southwestern China. Plateau Meteorology,40(4): 789-800. https://doi.org/10.7522/j.issn.1000-0534.2020.00048.(In Chinese).